All Theses and Dissertations (ETDs)

1-1-2012

Computational Fluid Dynamics (CFD) Modeling of Mixed Convection Flows in Building Enclosures

Alexander Kayne

Follow this and additional works at: https://openscholarship.wustl.edu/etd

WASHINGTON UNIVERSITY IN ST. LOUIS

School of Engineering and Applied Science

Department of Mechanical Engineering & Materials Science

Thesis Examination Committee:
Ramesh K. Agarwal (Chair)
David A. Peters
Harry Brandon

COMPUTATIONAL FLUID DYNAMICS (CFD) MODELING OF MIXED

CONVECTION FLOWS IN BUILDING ENCLOSURES

by

Alexander Kayne

A thesis presented to the School of Engineering and Applied Science
of Washington University in St. Louis in partial fulfillment of the
requirements for the degree of

MASTER OF SCIENCE

April 2012
Saint Louis, Missouri

ABSTRACT OF THE THESIS

Computational Fluid Dynamics (CFD) Modeling of Mixed

Convection Flows in Building Enclosures

by

Alexander Kayne

Master of Science in Mechanical Engineering

Washington University in St. Louis, 2012

Research Advisor: Professor Ramesh K. Agarwal

In recent years Computational Fluid Dynamics (CFD) simulations are increasingly used to model the air circulation and temperature environment inside the rooms of residential and office buildings to gain insight into the relative energy consumptions of various HVAC systems for cooling/heating for climate control and thermal comfort. This requires accurate simulation of turbulent flow and heat transfer for various types of ventilation systems using the Reynolds-Averaged Navier-Stokes (RANS) equations of fluid dynamics. Large Eddy Simulation (LES) or Direct Numerical Simulation (DNS) of Navier-Stokes equations is computationally intensive and expensive for simulations of this kind. As a result, vast majority of CFD simulations employ RANS equations in conjunction with a turbulence model. In order to assess the modeling requirements (mesh, numerical algorithm, turbulence model etc.) for accurate simulations, it is critical to validate the calculations against the experimental data. For this purpose, we use three well known benchmark validation cases, one for natural convection in 2-D closed vertical cavity, second for forced convection in a 2-D rectangular cavity and the third for mixed convection in a 2-D square cavity. The simulations are performed on a number of meshes of different density using a number of turbulence models. It is found that k-ε two-equation turbulence model with a second-order algorithm on a reasonable mesh gives the best results. This information is then used to determine the modeling requirements (mesh, numerical algorithm, turbulence model etc.) for

flows in 3D enclosures with different ventilation systems. In particular two cases are considered for which the experimental data is available. These cases are (1) air flow and heat transfer in a naturally ventilated room and (2) airflow and temperature distribution in an atrium. Good agreement with the experimental data and computations of other investigators is obtained.

Acknowledgments

I would like to thank my thesis advisor Dr. Ramesh Agarwal for his advice and guidance throughout this research. I would also like to thank the thesis committee members Dr. David Peters and Dr. Harold Brandon for reading the thesis and offering some constructive comments. Finally, I would like to acknowledge the help of my colleagues Travis Cocke and Tudor Foote in the CFD laboratory.

Alexander Kayne

Washington University in St. Louis
May 2012

Dedicated to my parents, William and Saundra Kayne.

Contents

List of Figures

List of Tables

Chapter 1

Introduction

1.1 Motivation

In the past decade, environmental concerns and the rising cost of energy have created a shift in building architecture towards more energy-efficient designs. The primary environmental concern has been the increase in greenhouse gases, due to the increasing fossil fuel consumption for electricity generation and transportation. Since buildings are major consumers of energy for heating, cooling, lighting, etc., an increase in energy efficiency of buildings contribute towards a significant decrease in emissions.

In 2009, buildings were the second-largest energy-consuming sector in the United States (Figure 1.1), using up to 33.9% of the nation's total energy consumption. Buildings also represented 77.8% of the nation's electrical energy consumption (Figure 1.2), 44.4% of which is generated through coal combustion (Figure 1.3). Coal combustion accounted for 34.6% of the nation's carbon dioxide emissions (Figure 1.4), and thus for 28.2% of the nation's overall greenhouse gas emissions (Figure 1.5). Therefore, to reduce greenhouse gas emissions, there has been an emphasis on increasing the energy efficiency of buildings. Heating, ventilation and air conditioning (HVAC) has become an integral part of all buildings across the nation; the space conditioning now takes up to 53% of the energy consumption by the end user in the residential sector (Peréz-Lombard et al., 2008). As a result, there is focus on reducing HVAC consumption as well as increasing its efficiency.
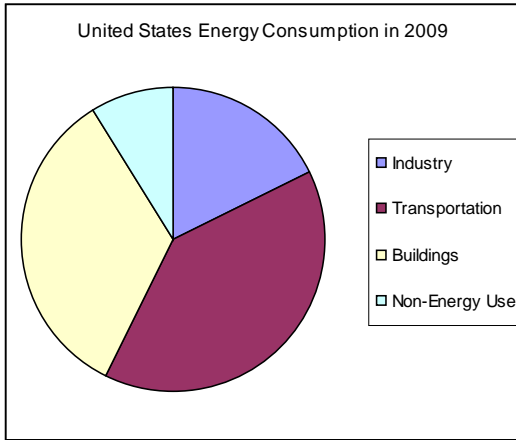
Fig. 1.1 United States Energy Usage by Sector [International Energy Agency (11)]
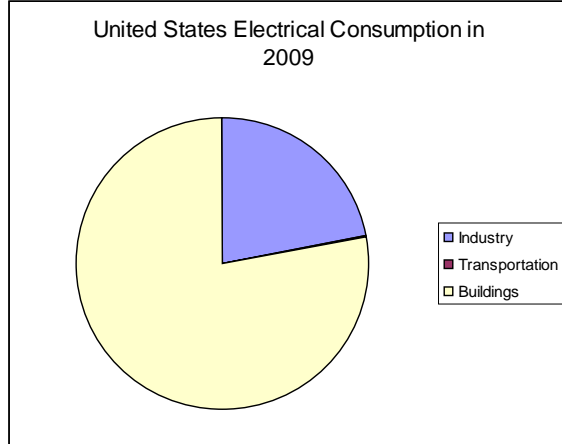
Fig. 1.2 United States Electrical Energy Usage by Sector [International Energy Agency (11)
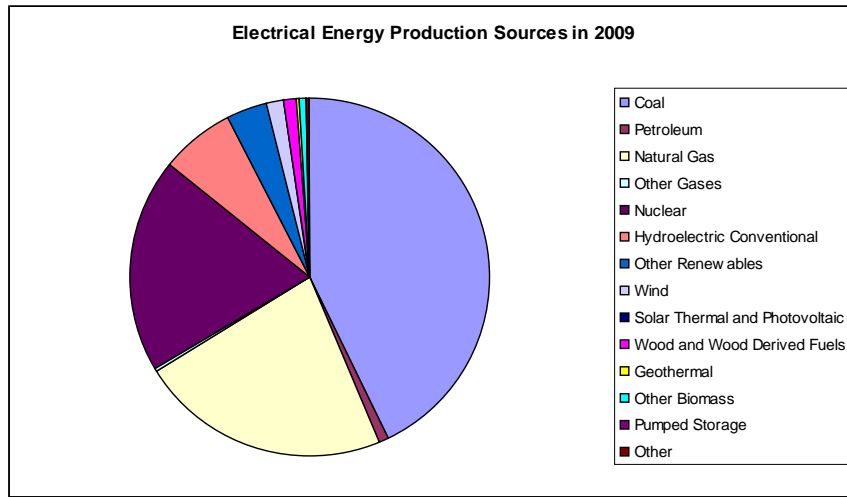
Fig. 1.3: United States Electrical Energy Production Sources in 2009 [Energy Information Administration (11)]
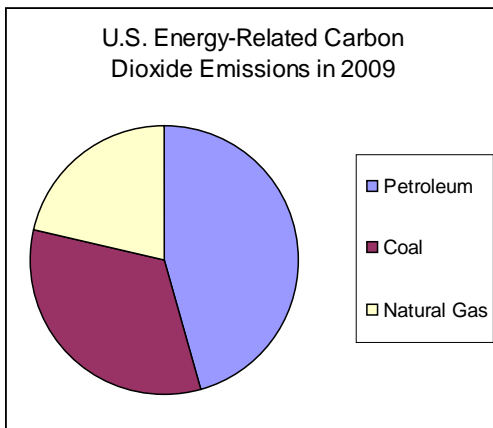
Fig. 1.4 U.S. Energy-Related Carbon Dioxide Emissions in 2009 [Environmental Protection Agency (18)]
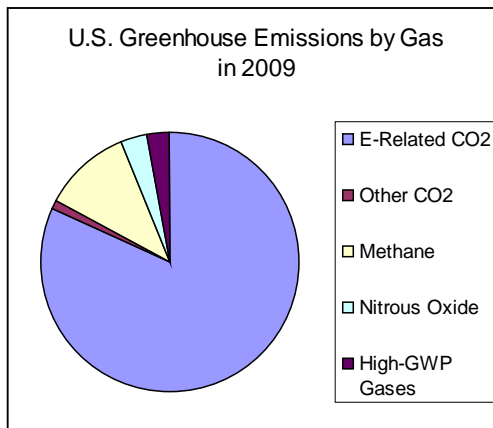
Fig. 1.5: U.S. Greenhouse Emissions by Gas in 2009 [U.S. Energy Information Administration (17)]

1.2 HVAC Modeling

Thanks to significant improvements in technology over the past several decades, HVAC is no longer considered a luxury but a basic need in most of the industrialized countries in the world. Considering that the average person in the United States spends over 90% of his life indoors (U.S. EPA 1995), coupled with the realization that goods are "produced better, faster, and more economically in a properly controlled environment" (McQuiston, Parker and Spitler 2005), HVAC has become a vital need for both the health and productivity of the people worldwide.

Because buildings in different regions of the United States and the world have different heating, cooling and ventilation requirements, it is impossible to create a single energy-efficient and economical HVAC system that can be applied to every building. This can be seen in the balkanization of HVAC industries and materials, in which everything from design to position to setting must be carefully chosen for optimal effect. To the design of energy-efficient HVAC systems and to assess and improve the energy efficiency of buildings, building architects and the HVAC industry are increasingly employing flow and heat transfer modeling software to study the flow field in building enclosures and the impact of various HVAC systems on the thermal comfort.

1.3   Scope of the Thesis

The main objective of the research conducted in this thesis is to study the flow field and heat transfer in 3D building enclosures using computational fluid dynamics (CFD) software. For this purpose, the CFD software from ANSYS Inc., called FLUENT 12.1, is employed. The software is first employed to study the flow field in 2-D enclosures for the purpose of code validation and for determining the numerical requirements (mesh, algorithm accuracy, etc.) for accurate simulations. Three cases for which experimental data is available are studied. These cases are:

- A 2-D rectangular cavity with forced convection

- A 2-D vertical "tall cavity" with natural convection

- A 2-D square cavity with mixed convection (combined forced and natural convection)

After code validation with 2-D cases, flow fields in two 3D enclosures are computed. These cases are:

- A 3-D room with a single heater with natural ventilation

- A 3-D atrium with both mixed convection and solar radiation (from a single external glass wall)

In the CFD calculations using FLUENT, we employ the Reynolds Averaged Navier-Stokes (RANS) equations. Because of the relatively low airspeed in each case, we apply the incompressible form of the equations with the Boussinesq Approximation to account for the buoyancy effects. In all the studies, the computations are performed on a sequence of meshes to ascertain that the final solution is mesh-independent. In addition, several turbulence models, in particular the two-equation k-ε realizable and k-ω SST models, are employed to assess the effect of turbulence models on the accuracy of the solutions.

Chapter 2

Background Theory and Modeling

2.1 Introduction

Computational Fluid Dynamics (CFD) is a numerical approach for simulating fluid flow. It allows the practitioners and researchers to predict characteristics of a system, including flow velocity, pressure, temperature and heat transfer. CFD analysis takes place in three stages:

First, a pre-processing application (in the present work, ANSYS GAMBIT) is used to establish the geometry of the model. Boundaries (such as walls, inlets and outlets) are also defined in this step. When the geometry and the boundary conditions for the problem are completed, the computational domain in defining the problem is divided into quadrilateral or triangular cells in 2-D; or hexagonal or tetrahedral cells in 3D, which form a mesh or a grid. This mesh is then imported to ANSYS FLUENT 12.1 for generating the flow field solutions at mesh points.

It is important that proper boundary conditions such as wall temperature, inlet velocity and gauge pressure are applied in the computational domain.

The CFD Solver FLUENT generates the flow field data at each mesh point after solving the appropriate governing equations. After the flow field is generated by FLUENT, it is exported to a data processor (in the present work, CFD-Post) to generate line plots and flow variable contours. This data can also be exported to other software such as Excel to allow comparisons with the other calculations and data in a straightforward manner.

2.2   Fundamentals of CFD

The use of computational flow dynamics (CFD) is a numerical methodology for solving the governing equations of fluid flow. The governing equations of fluid flow are partial differential equations; when discretized on a mesh, they transform into algebraic equations which can be solved by a finite-difference/finite-volume algorithm (Basarir 2009).

The following sections will briefly describe the governing equations, turbulence models, flow conditions and properties employed in this work.

2.3   Governing Equations

For a Newtonian fluid, the governing equations of fluid flow describing the conservation of mass, momentum and energy in Cartesian coordinate systems can be written as follows (Currie, 2003):

Conservation of Mass

$$\frac{\partial \rho}{\partial t} + \frac{\partial (\rho u)}{\partial x} + \frac{\partial (\rho v)}{\partial y} + \frac{\partial (\rho w)}{\partial z} = 0 \tag{2.1}$$

Conservation of Momentum

We choose the y-coordinate to be in the vertical direction opposite to the direction ingravity. The buoyancy forces act in the y-direction. The conservation of momentum equations in the Cartesian coordinates can be written as:

x-Momentum Equation

$$\frac{\partial}{\partial t}(\rho u) + \frac{\partial}{\partial x}(\rho uu) + \frac{\partial}{\partial y}(\rho vu) + \frac{\partial}{\partial z}(\rho wu) = -\frac{\partial P}{\partial x} + \mu(\frac{\partial^2 u}{\partial x^2} + \frac{\partial^2 u}{\partial y^2} + \frac{\partial^2 u}{\partial z^2}) \tag{2.2}$$

y-Momentum Equation

$$\frac{\partial}{\partial t}(\rho v) + \frac{\partial}{\partial x}(\rho uv) + \frac{\partial}{\partial y}(\rho vv) + \frac{\partial}{\partial z}(\rho wv) =$$
$$-\frac{\partial P}{\partial y} + \mu(\frac{\partial^2 w}{\partial x^2} + \frac{\partial^2 w}{\partial y^2} + \frac{\partial^2 w}{\partial z^2}) - \rho g \beta (T_\infty - T) \tag{2.3}$$

6

z-Momentum Equation

$$\frac{\partial}{\partial t}(\rho w) + \frac{\partial}{\partial x}(\rho u w) + \frac{\partial}{\partial y}(\rho v w) + \frac{\partial}{\partial z}(\rho w w)$$

$$= -\frac{\partial P}{\partial z} + \mu(\frac{\partial^2 w}{\partial x^2} + \frac{\partial^2 w}{\partial y^2} + \frac{\partial^2 w}{\partial z^2}) \tag{2.4}$$

Conservation of Energy

$$\frac{\partial}{\partial t}(\rho c_p T) + \frac{\partial}{\partial x}(\rho u c_p T) + \frac{\partial}{\partial y}(\rho v c_p T) + \frac{\partial}{\partial z}(\rho w c_p T)$$

$$= k(\frac{\partial^2 T}{\partial x^2} + \frac{\partial^2 T}{\partial y^2} + \frac{\partial^2 T}{\partial z^2}) + q'' \tag{2.5}$$

2.4   Turbulence Modeling

2.4.1 Reynolds Averaged Navier-Stokes Equations

Direct numerical simulation (DNS) of the governing equations described in Section 2.3 is not feasible at present for complex 3D problems at high-Reynolds numbers, because very large computational hardware requirements are presently unavailable. Although Large-Eddy Simulation (LES) is relatively less computationally intensive, it is still impractical for many three-dimensional applications. As a result, a majority of the turbulent flows are computed by time-averaging the equations of Section 2.3. This is done by replacing the instantaneous quantities in Equations (2.1)-(2.5) by the sum of their mean and fluctuating parts. For example, $u = \bar{u} + u'$, where u is the time-mean quantity and u' is the instantaneous fluctuating quantity (Cebeci and Cousteix, 2005). Performing these substitutions and invoking time-averaging Equations (2.1)-(2.5) transforms them into the well-known Reynolds Averaged Navier-Stokes (RANS) Equations:

Conservation of Mass

$$\frac{\partial(\rho \bar{u})}{\partial x} + \frac{\partial(\rho \bar{v})}{\partial y} + \frac{\partial(\rho \bar{w})}{\partial z} = 0 \tag{2.6}$$

Conservation of Momentum

x-Momentum Equation

$$\frac{\partial}{\partial t}(\rho\overline{u}) + \frac{\partial}{\partial x}(\rho\overline{u}\,\overline{u}) + \frac{\partial}{\partial y}(\rho\overline{v}\,\overline{u}) + \frac{\partial}{\partial z}(\rho\overline{w}\,\overline{u})$$

$$= -\frac{\partial\overline{P}}{\partial x} + (\mu + \mu_t)(\frac{\partial^2\overline{u}}{\partial x^2} + \frac{\partial^2\overline{u}}{\partial y^2} + \frac{\partial^2\overline{u}}{\partial z^2})$$

(2.7)

y-Momentum Equation

$$\frac{\partial}{\partial t}(\rho\overline{v}) + \frac{\partial}{\partial x}(\rho\overline{u}\,\overline{v}) + \frac{\partial}{\partial y}(\rho\overline{v}\,\overline{v}) + \frac{\partial}{\partial z}(\rho\overline{w}\,\overline{v}) =$$

$$-\frac{\partial\overline{P}}{\partial y} + (\mu + \mu_t)(\frac{\partial^2\overline{w}}{\partial x^2} + \frac{\partial^2\overline{w}}{\partial y^2} + \frac{\partial^2\overline{w}}{\partial z^2}) - \rho g\beta(T_\infty - T)$$

(2.8)

z-Momentum Equation

$$\frac{\partial}{\partial t}(\rho\overline{w}) + \frac{\partial}{\partial x}(\rho\overline{u}\,\overline{w}) + \frac{\partial}{\partial y}(\rho\overline{v}\,\overline{w}) + \frac{\partial}{\partial z}(\rho\overline{w}\,\overline{w})$$

$$= -\frac{\partial\overline{P}}{\partial z} + (\mu + \mu_t)(\frac{\partial^2\overline{w}}{\partial x^2} + \frac{\partial^2\overline{w}}{\partial y^2} + \frac{\partial^2\overline{w}}{\partial z^2})$$

(2.9)

Conservation of Energy

$$\frac{\partial}{\partial t}(\rho c_p\overline{T}) + \frac{\partial}{\partial x}(\rho\overline{u}c_p\overline{T}) + \frac{\partial}{\partial y}(\rho\overline{v}c_p\overline{T}) + \frac{\partial}{\partial z}(\rho\overline{w}c_p\overline{T}) =$$

$$k(\frac{\partial^2\overline{T}}{\partial x^2} + \frac{\partial^2\overline{T}}{\partial y^2} + \frac{\partial^2\overline{T}}{\partial z^2}) + \frac{\partial}{\partial x_t}(\frac{\partial\overline{T}}{\partial x_t}\frac{c_p\mu_t}{\sigma_t}) + q''$$

(2.10)

As a result of Reynolds-averaging, Reynolds stresses appear in Equations (2.7)-(2.9) that need to be modeled. They are modeled in an analogous manner as the laminar stress terms μ_t (known as the eddy viscosity). There has been considerable effort devoted over the last hundred years towards the modeling of μ_t. This practice is known as "turbulence modeling." In the next two sections, we briefly describe the two models we have employed in this thesis.

2.4.2   The k-ε Turbulence Model

The k-ε model is based on determining μ_t by solving two transport equations, one for the turbulent kinetic energy k and the other for the rate of dissipation of turbulent kinetic energy ε. Eddy viscosity is determined by the equation $\mu_t = \rho C_\mu \dfrac{k^2}{\varepsilon}$. In the realizable k-ε equations, the Boussinesq approximation in the Reynolds Stress in an incompressible strained-mean flow become:

$$\frac{\partial}{\partial t}(\rho k) + \frac{\partial}{\partial x_j}(\rho k u_i) = \frac{\partial}{\partial x_j}[(\mu + \frac{\mu_t}{\sigma_k})\frac{\partial k}{\partial x_j}] + G_k + G_b - \rho\varepsilon - Y_M + S_k \qquad (2.11)$$

$$\frac{\partial}{\partial t}(\rho\varepsilon) + \frac{\partial}{\partial x_j}(\rho\varepsilon u_j) =$$

$$\frac{\partial}{\partial x_j}[(\mu + \frac{\mu_t}{\sigma_\varepsilon})\frac{\partial\varepsilon}{\partial x_j}] + \rho C_1 S\varepsilon - \rho C_2 \frac{\varepsilon^2}{k + \sqrt{\upsilon\varepsilon}} + C_{1\varepsilon}\frac{\varepsilon}{k}C_{3\varepsilon}G_b + S_\varepsilon \qquad (2.12)$$

where G_k represents the generation of turbulence kinetic energy due to mean velocity gradients, G_b is the generation of turbulence kinetic energy due to buoyancy, Y_m represents the contribution of the fluctuation dilation in compressible turbulence to the overall dissipation rate, S_k and S_ε are user-defined source terms, σ_ε and σ_k are the Prandtl numbers for k and ε respectively, and $C_{1\varepsilon}$ and C_2 are constants. ANSYS FLUENT 12.1 has established the latter four terms to ensure that the model performs well for canonical flows. The model's constants are given as:

$C_{1\varepsilon} = 1.44$, $C_2 = 1.9$, $\sigma_k = 1.0$, and $\sigma_\varepsilon = 1.2$, \qquad (2.13)

which work well for a wide range of wall-bounded and free shear flows (FLUENT, 2009).

2.4.3 The k-ω Turbulence Model

The k-ω model is based on the transport equations for the turbulence kinetic energy k and the specific dissipation rate ω. The k-ω model is supposedly "more accurate than k-ε in the near wall layers, and has therefore been successful for flows with more moderate adverse pressure gradients, but fails for flows with pressure-induced

separation" (Menter, Kuntz and Langry, 2003). Thanks to the Wilcox Shear-Stress Transport modification, k-ω is widely used in industrial, commercial and research codes; however, because of its free-stream sensitivity to the values of ω, it has yet to overtake k-ε in popularity. The transport equations for k and ω are given as:

$$\frac{\partial(\rho k)}{\partial t} + \frac{\partial(\rho u_i k)}{\partial x_i} = \frac{\partial}{\partial x_j}(\Gamma_k \frac{\partial k}{\partial x_j}) + \tilde{G}_k - Y_k + S_k \tag{2.14}$$

$$\frac{\partial(\rho \omega)}{\partial t} + \frac{\partial(\rho u_i \omega)}{\partial x_i} = \frac{\partial}{\partial x_j}[\Gamma_\omega \frac{\partial \omega}{\partial x_j}] + G_\omega - Y_\omega + D_\omega + S_\omega \tag{2.15}$$

where Γ_k and Γ_ω represents the effective diffusivities, S is the strain rate magnitude, $\check{G}_k$ represents the generation of turbulence kinetic energy due to mean velocity gradients, G_ω represents the generation of ω, Y represents the dissipation of its respective variable due to turbulence, S_k and S_ω are user defined source terms, and D_w is the representative cross-diffusion term

$$D_\omega = 2(1 - F_1)\rho \sigma_{\omega,2} \frac{1}{\omega} \frac{\partial k}{\partial x_j} \frac{\partial \omega}{\partial x_j} \tag{2.16}$$

where F_1 is the blending function and $\sigma_{w,2} = 1.168$.

2.5   Radiation Modeling

In addition to both natural and forced convection, one of the 3D cases studied in this thesis includes solar radiation. To account for the effects of solar radiation, the Discrete Transfer Radiation Model (DTRM) built in FLUENT is employed. This model solves the Radiation Intensity equation

$$\frac{dI}{ds} + aI = \frac{a\sigma T^4}{\pi} \tag{2.17}$$

by integrating it along a series of rays s coming from the faces of the radiating body. So long as the gas absorption coefficient a is constant, the intensity $I(s)$ can be estimated as

$$I(s) = \frac{\sigma T^4}{\pi}(1 - e^{-as}) + I_0 e^{-as} \tag{2.18}$$

where σ is the Stefan-Boltzmann constant, T is the temperature, and I_0 is the radiant intensity at the beginning of the path given by the equation

$$I_0 = \frac{(1 - e_w)q_{in} + e_w \sigma T_w^4}{\pi}$$
(2.19)

In Equation (2.19), q_{in} is the radiative heat flux entering the wall from the surroundings and e_w and T_w are the wall emissivities and temperatures, respectively (FLUENT 2009).

2.6   Numerical Solution Method

The RANS equations and turbulence models (as well as the radiative transfer model) create a system of seven equations that need to be solved numerically. An analytical solution for these equations is impossible; therefore, an iterative numerical solution method is used on a mesh to approximate the partial differential equations into of approximate algebraic equations. The linearized algebraic equations iteratively converge to the nonlinear solutions by employing a suitable algorithm built in FLUENT. A convergence criteria is specified to achieve an acceptable accuracy. When all the flow properties in all cells of the mesh reach the convergence criteria, the solution is considered "converged" and the iterative process ends (Basarir 2009).
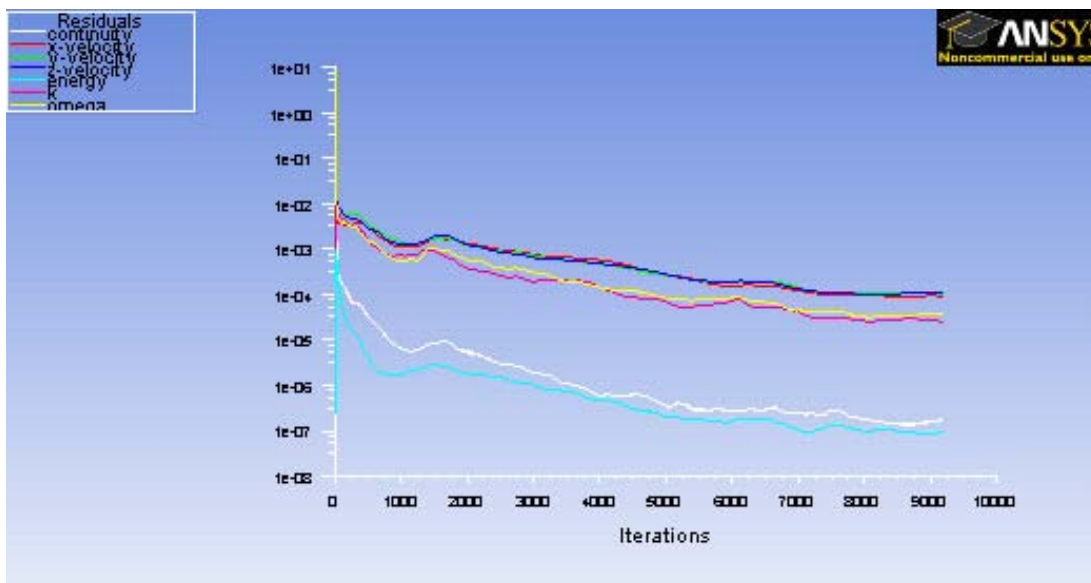
Fig. 2.1 Example of Residual History of Various Flow Variables and Governing Equations During the Iterative Process

11

2.7   Solver Settings

The choice of solver settings in FLUENT has been based on existing literature and guidelines for modeling of large air spaces (Cornell 2011).

The following solver settings were used in all the 2-D and 3D cases studied in this thesis except for the 3D Atrium case:

- Double Precision, Segregated Steady Solver
- Standard Method for Pressure
- Second Order Upwind Discretization for Momentum, Turbulence and Energy Equations
- Under-relaxation factors for pressure, density, body forces, momentum, turbulent kinetic energy, turbulent dissipation rate, turbulent viscosity and energy are equal to 0.3, 1, 1, 0.7, 0.8, and 1 respectively
- SIMPLE! Algorithm with Pressure-Velocity Coupling
- Convergence criteria of 0.000001

In the final (Atrium) case, in order to be able to compare the results with those of (Basarir 2009), the Body-Force Weighted method was chosen for solving for pressure and the convergence criteria was relaxed to 0.0001.

2.8   Assumptions for Validation Cases

The following fluid properties were used for the 2-D validation cases:
- Newtonian Fluid (Air)
- Steady-State
- Two-Dimensional

- Bousinessq Approximation for buoyancy forces, which states that in buoyancy-driven flows, variation in density may be neglected in the continuity equation and should be included only in the direction of gravity (Currie, 2003). The density changes only with temperature in the buoyancy term in the y-momentum equation.
- Gravitational acceleration acting in the negative y-direction at a rate of 9.81 m/s^2
- Adiabatic Walls
- Density of Air = 1.204 kg/m^3
- Specific Heat of Air = 1006.43 J/kg-K
- Thermal Conductivity of Air = 0.0242 W/m-K
- Viscosity of Air = 1.825 x 10^{-5} kg/m-s
- Thermal Expansion Coefficient of Air = 0.0017884 1/K

Chapter 3

Simulation of Forced Convection in a 2-D Rectangular Cavity

3.1   2-D Model

The 2-D model employed to study the forced convection on a rectangular cavity was studied experimentally by Restivo (1979). In this model, the rectangular cavity is of height H = 3 m and length L = 9 m. An inlet slot with height h = 0.168 *m* is made near the upper wall of the cavity, and an outlet slot for air is made near the wall bottom with a height t = 0.48 m. A steady airflow is forced into the cavity chamber at 0.455 m/s, introducing circulation into the room. The incoming air has a Reynolds Number of 5000, based on the inlet size, inlet velocity and ambient air conditions. It induces turbulent flow in the chamber. Experiments of Restivo (1979) measured the streamwise (*u*) velocity along the vertical axis at x = 3 m and x = 2 m, and along the horizontal axis at y = 0.084 m and y = 2.916 m. Results from our study are presented along with the computational results of by Horikiri, Yao and Yao (2011), and by De Villiers (2010).
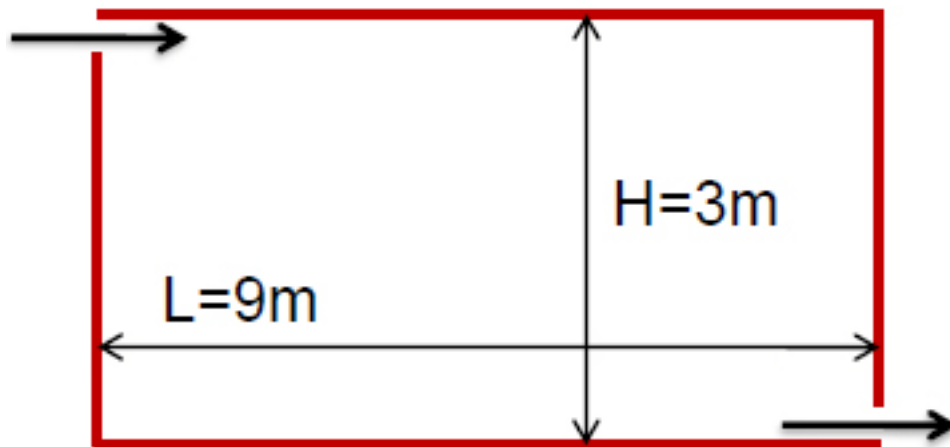
Fig. 3.1 Sketch of the 2-D Forced Convection Model [de Villiers 2010 (8)]

In addition to the goal of validation of CFD solvers for computing forced convection flows, one of the key focuses of this study was to determine the effect of mesh density and turbulence models on the accuracy of the results. For this purpose, six cases were computed. Computations were performed for mesh spacings of 0.05, 0.01 and 0.005 for both k-ε realizable and k-ω SST models. These meshes resulted in 10800, 270000 and 1080000 nodes.

3.2   Results and Discussion

Figure 3.2 shows the comparison of our results from three mesh spacings of 0.05 m, 0.01 m, and 0.005 m using the k-ω SST model with the experimental flows of Restivo (1979) and the computations of Horiki, Yao and Yao (2011) along the line x = 3.

Figure 3.3 shows the comparison of our results from three mesh spacings of 0.05 m, 0.01 m, and 0.005 m using the k-ω SST model with the experimental results of Restivo (1979) and the computations of Horikiri, Yao and Yao (2011) along the line x = 6.

From Figures 3.2 and 3.3, it can be seen that the agreement between computation and experiment improves between x = 0.7 and x = 3; the discrepancy is larger near the wall between x = 0 and x = 0.7. It can also be noted that coarser meshes made with a spacing of 0.05 m give poor results. Best results with reasonable computational time are obtained on a mesh of 0.01 m spacing and use of the k-ε realizable turbulence model. Further refinement of mesh spacing to 0.005 m increases the computational time significantly without significant impact on accuracy. Also, the k-ω SST turbulence model gives less accurate results when compared to the k-ɛ realizable model, especially near the vertical walls.

Figure 3.4 shows the computed velocity vectors inside the cavity obtained with the k-ε model. A large region of recirculating flow can be seen near the left wall, as expected.
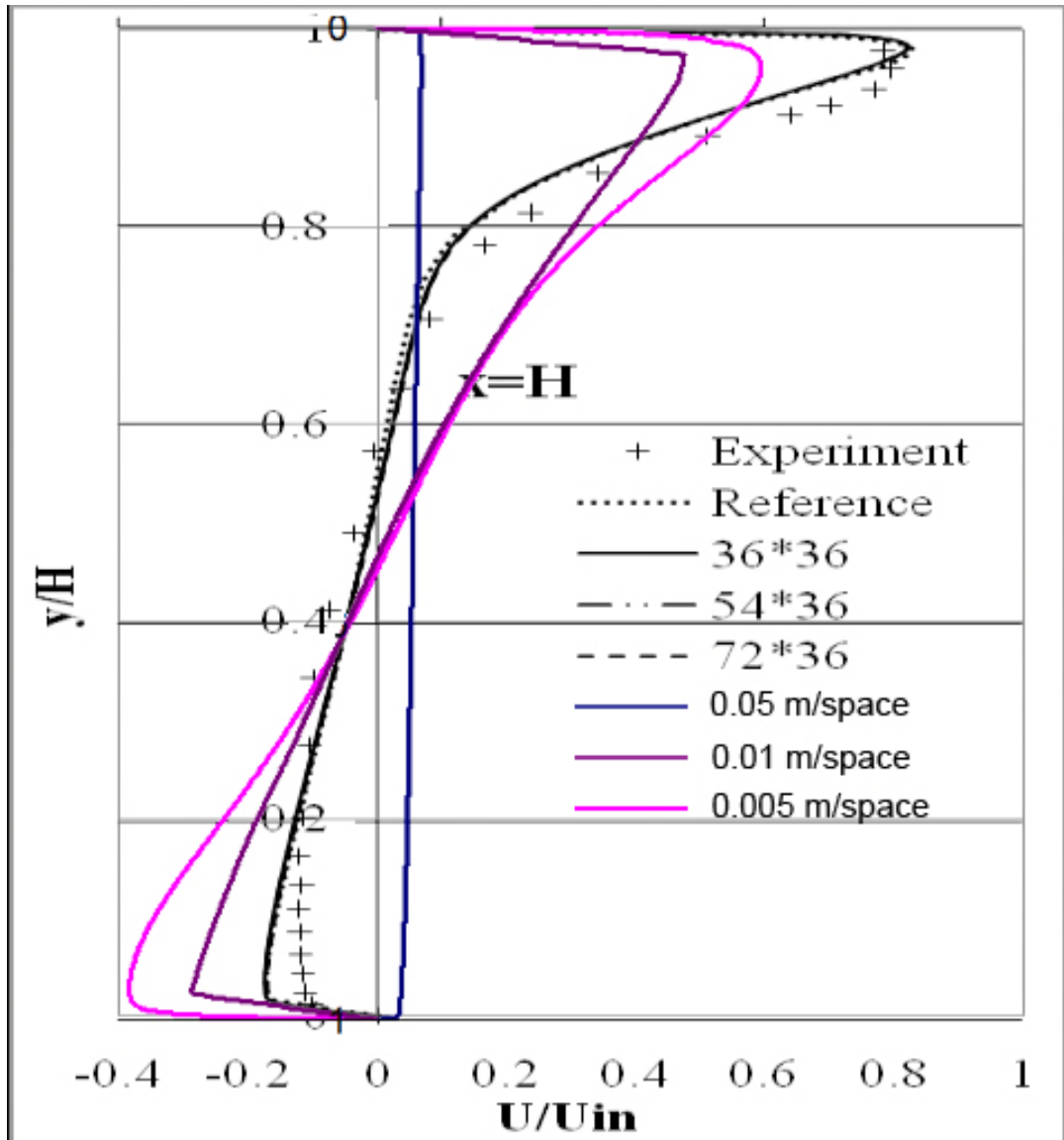
Present Results for Three Different Mesh Spacings with Experimental Data of [Restivo 1979 (16)] and the Computations of [Horikiri, Yao and Yao 2011 (11)] at x = 3 Using the k-ω Turbulence Model
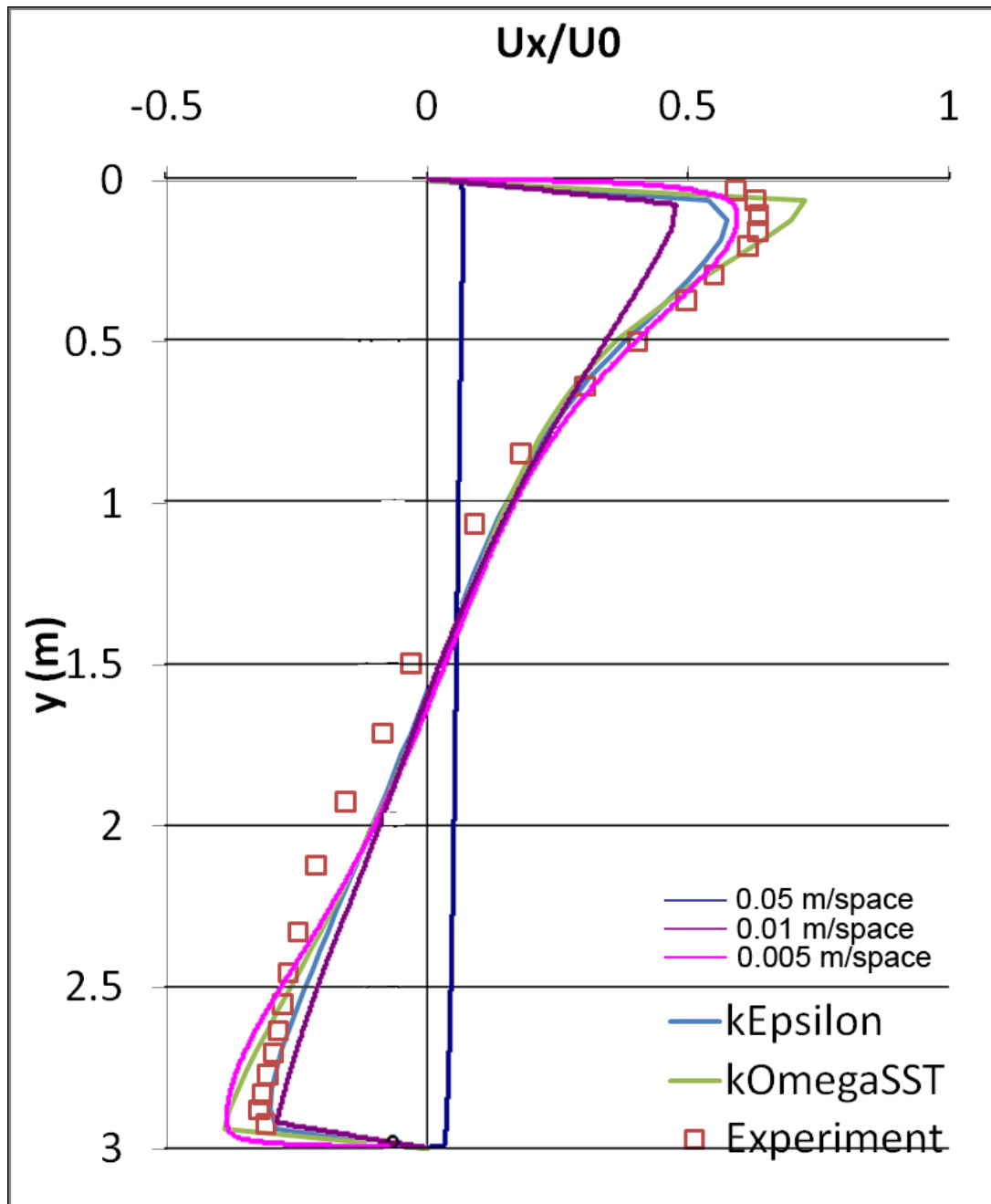
Present Results for Three Different Mesh Spacings with Experimental Data of [Restivo 1979 (16)] and the Computations of [Horikiri, Yao and Yao 2011 (11)] at x = 6 Using the k-ω Turbulence Model
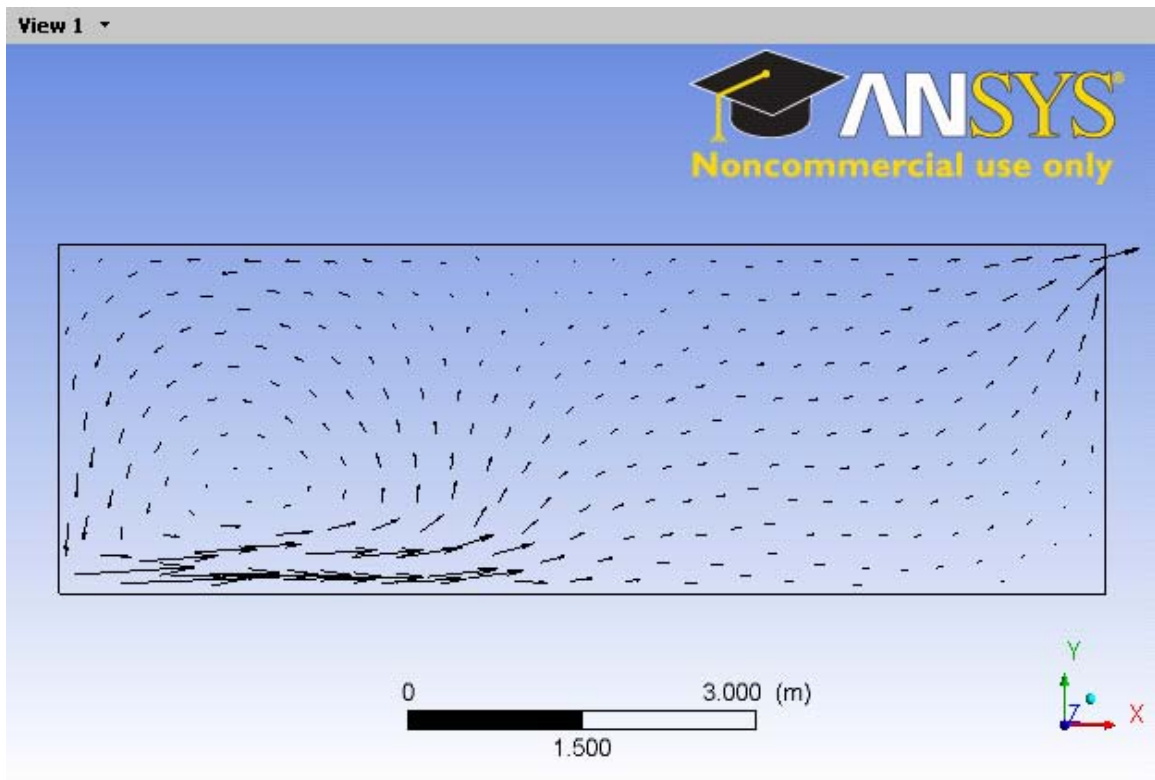
Fig. 3.4 Computed Velocity Vectors for Forced Convection in the Rectangular Cavity Using the k-ε Realizable Turbulence Model

After determining the appropriate mesh density for accurate simulations, we studied the influence of turbulence models on the accuracy of solutions. Figures 3.5 and 3.6 show the computed solutions with both the k-ω SST and k-ε realizable models on a mesh spacing of 0.008 m at x = 3 m and x = 6 m, respectively, and their comparisons with the experimental data of Restivo (1979) and the computations of De Villiers (2010). It can be seen from Figures 3.5 and 3.6 that the k-ε turbulence model gives a better agreement with the experimental data.

Figures 3.7 and 3.8 show the velocity profiles along the x-direction at y = 0.084 m and y = 2.916 m, respectively. Although in Figures 3.7 and 3.8 none of the models do a good job when compared with the data, the k-ε realizable turbulence model appears to be more accurate compared to the k-ω SST model.
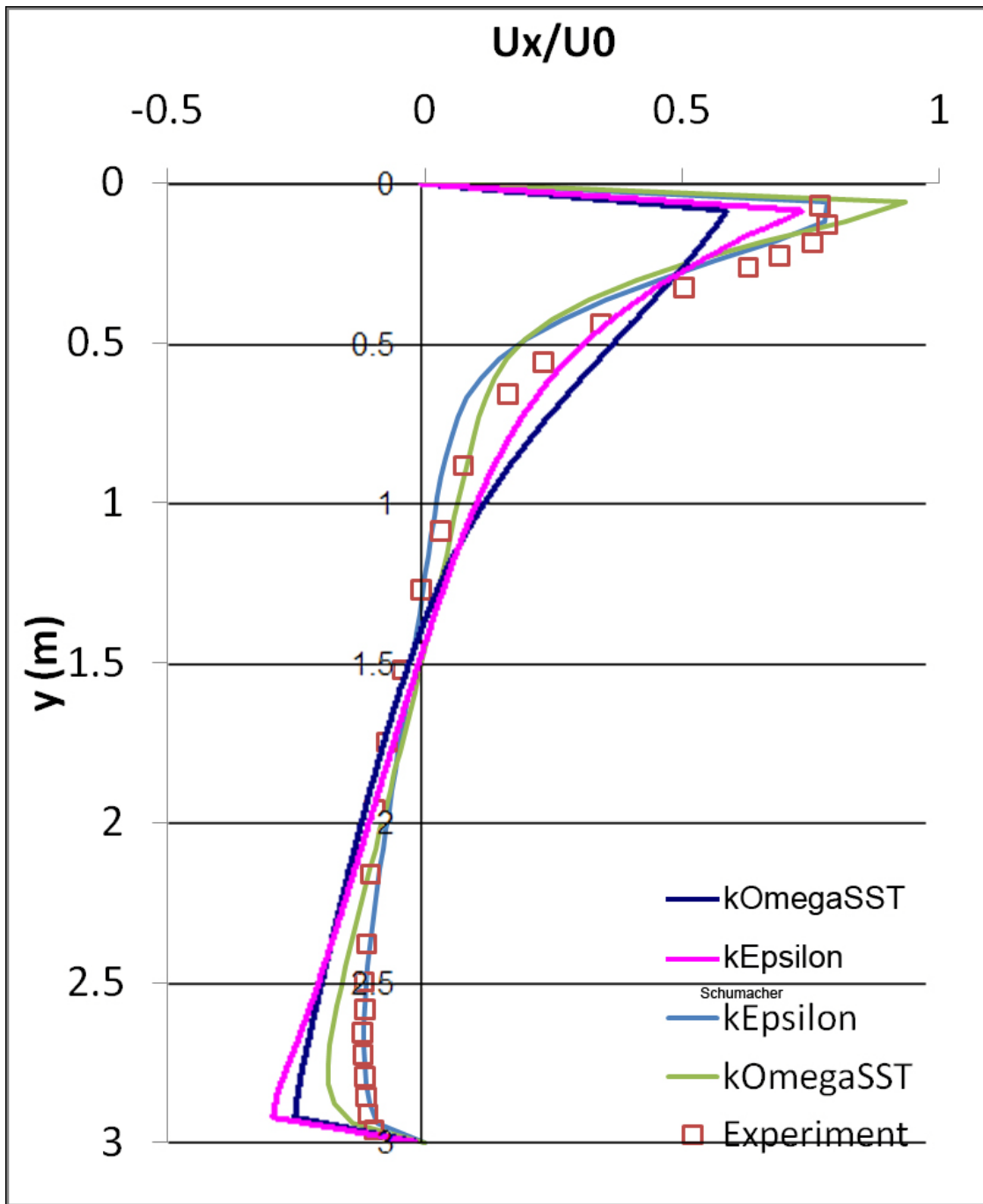
Fig. 3.5 Comparison of CFD Results With Experimental Data at x = 3 m [de Villiers 2010 (8)]
Using the k-ε Realizable and k-ω SST Turbulence Models
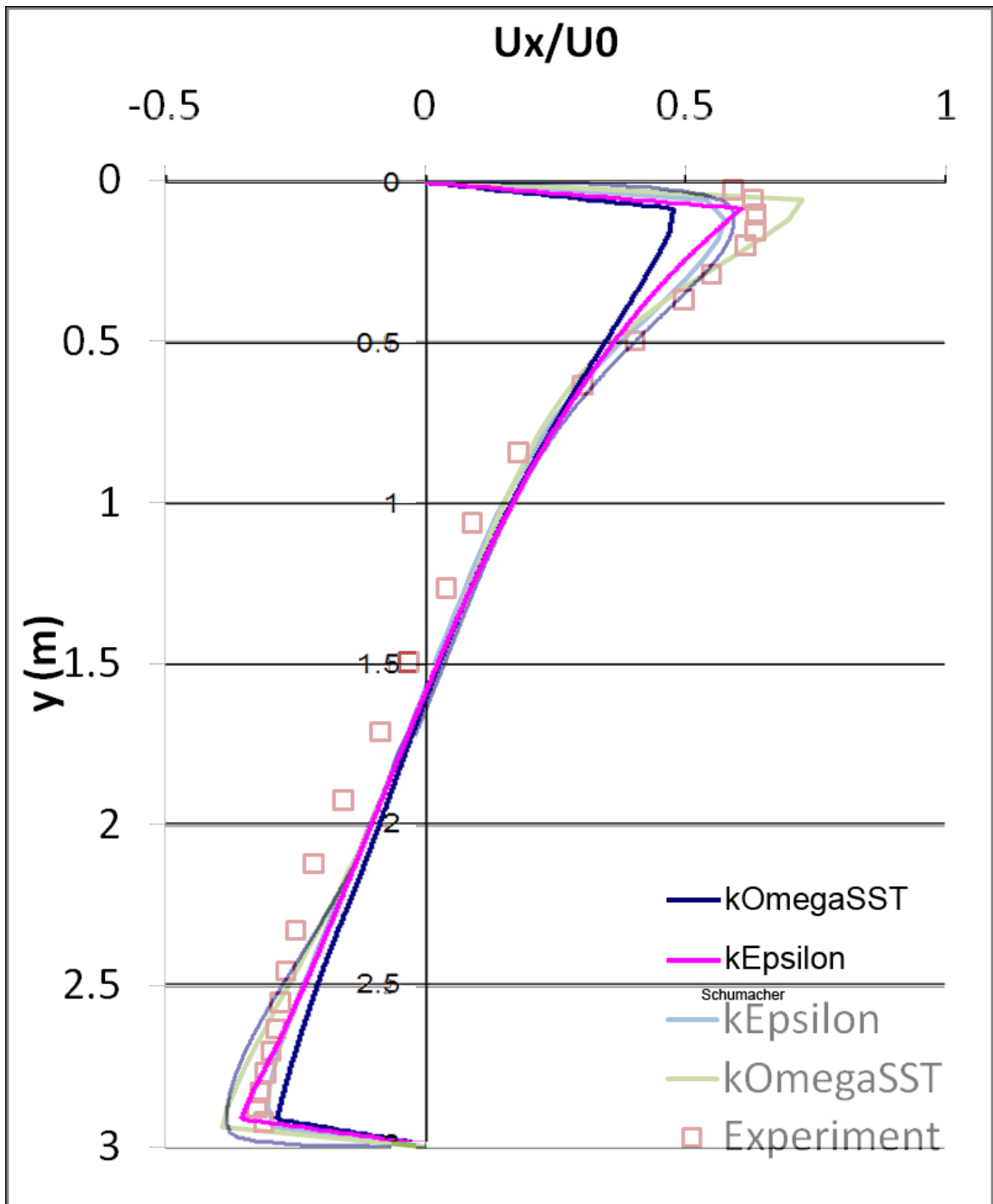
**Fig. 3.6 Comparison of CFD Results With Experimental Data at x = 6 m [de Villiers 2010 (8)]
Using the k-ɛ Realizable and k-ω SST Turbulence Models**
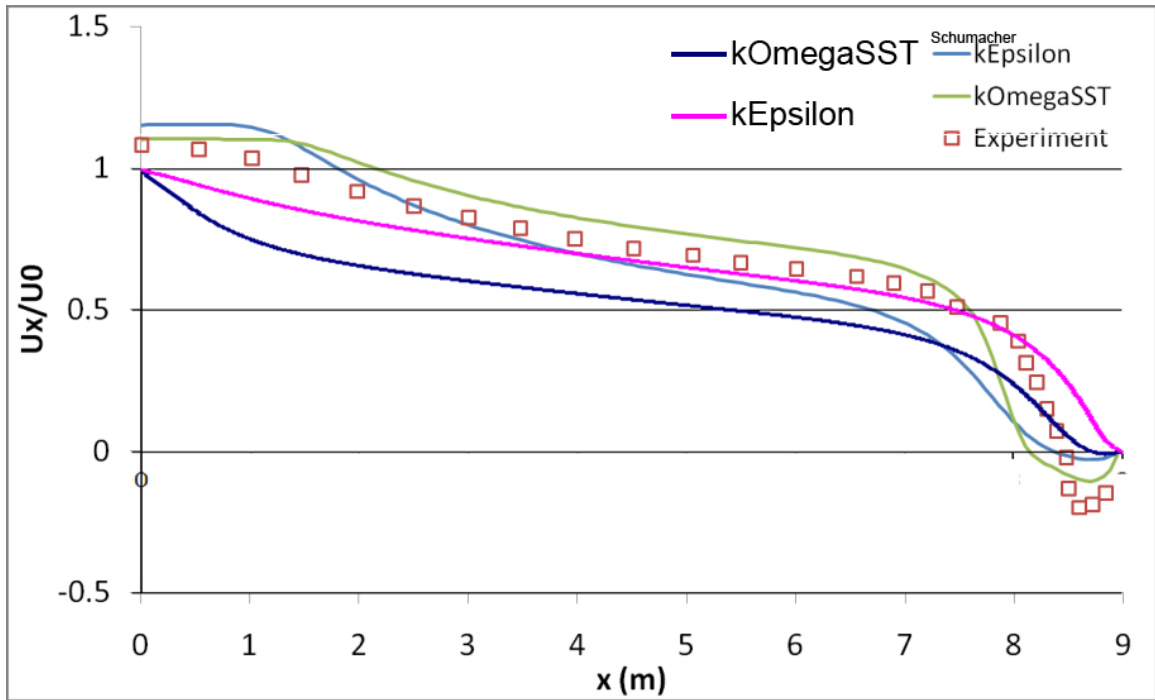
**Fig. 3.7 Comparison of CFD Results With Experimental Data at y = 0.084 m [de Villiers 2010 (8)]
Using the k-ε Realizable and k-ω SST Turbulence Models**
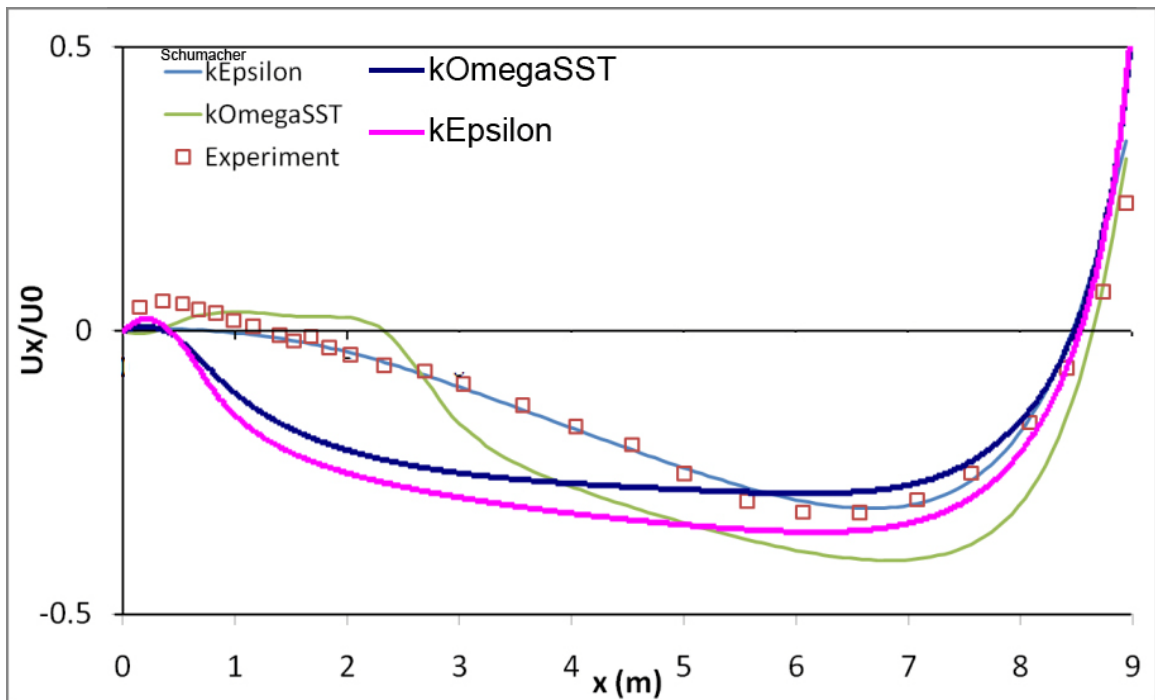
**Fig. 3.8 Comparison of CFD Results With Experimental Data at y = 2.916 m [de Villiers 2010 (8)]
Using the k-ε Realizable and k-ω SST Turbulence Models**

The simulations conducted in this chapter demonstrate that a suitable mesh spacing and k-ε realizable turbulence model can model the forced convection flow with acceptable engineering accuracy. It appears that better turbulence models are needed for more accurate prediction.

Chapter 4

Simulation of Natural Convection in a 2-D Vertical Rectangular Cavity

4.1 2-D Model

This model is based on an experimental study performed by P.L. Betts and I.H. Bokhari (2000). The model in their experiment (Figure 4.1) is a tall, hollow closed cavity with no inlets or outlets. The cavity has height H = 2.18 m, width W = 0.076 m, and depth D = 0.52 m. The vertical walls (closest to one another) are polished aluminum plates, one heated to 288.25 K and the other at 307.85 K. The top and bottom walls are assumed to be adiabatic. These boundary conditions correspond to a Rayleigh Number (*Ra*) of 8.6 x 10^5, defined as

$$Ra = \frac{g\beta(T_h - T_t)H^3}{va}$$

where $\underline{T_t}$ is the air temperature at the center of the cavity. Although the experiment was performed in 3-D, the enclosure in Fig. 4.1 can be modeled as nominally 2-D.

Having established in Chapter 3 that nearly 150000 to 700000 are sufficient to obtain reasonably accurate results, a mesh spacing of 0.001 was employed in this case for acceptable accuracy without excessively increasing computational time. The key goal of this study was to determine the relative accuracy of the two turbulence models for natural convection flow. Present computations are compared with the experimental data of Betts and Bokhari (2000) and the computations of Zuo and Chen (2009) and De Villiers (2010).
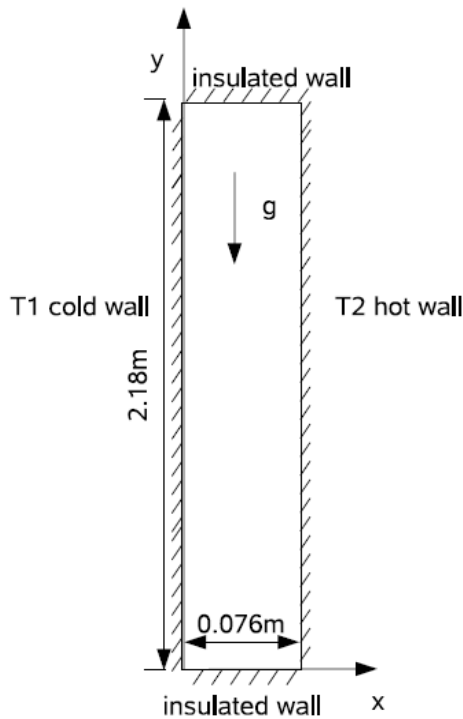
Fig. 4.1 Sketch of the 2-D Natural Convection Model [Zuo and Chen 2009 (20)]

4.2 Results and Discussion

Figures 4.2-4.7 show the comparison of present computations with the experimental data of Betts and Bokhari (2000) and with the computations of Zuo and Chen (2009) and de Villiers (2010) at various locations in the cavity for both the velocity and temperature profiles.

Unlike the Forced Convection case in Chapter 3, in this case the *k-ω* SST model gave more accurate results. While the realizable *k-ε* realizable model gave a reasonable prediction of temperature and velocity profiles in the De Villiers (2010) study, the *k-ω* SST model employed in the present study gives results in closer agreement with the experimental data, especially in capturing the velocity peaks at various x-locations. It also gave more accurate results for the velocity and temperature in the y-direction (y/H = 0.05, y/H = 0.1, y/h = 0.9, and y/h = 0.95), thus supporting the claim in the

24

literature that the k-ω SST turbulence model is superior in modeling the near-wall layers (Menter, Kuntz and Langry, 2003).

This case provides an excellent validation of the CFD solver for computing natural convection flows.
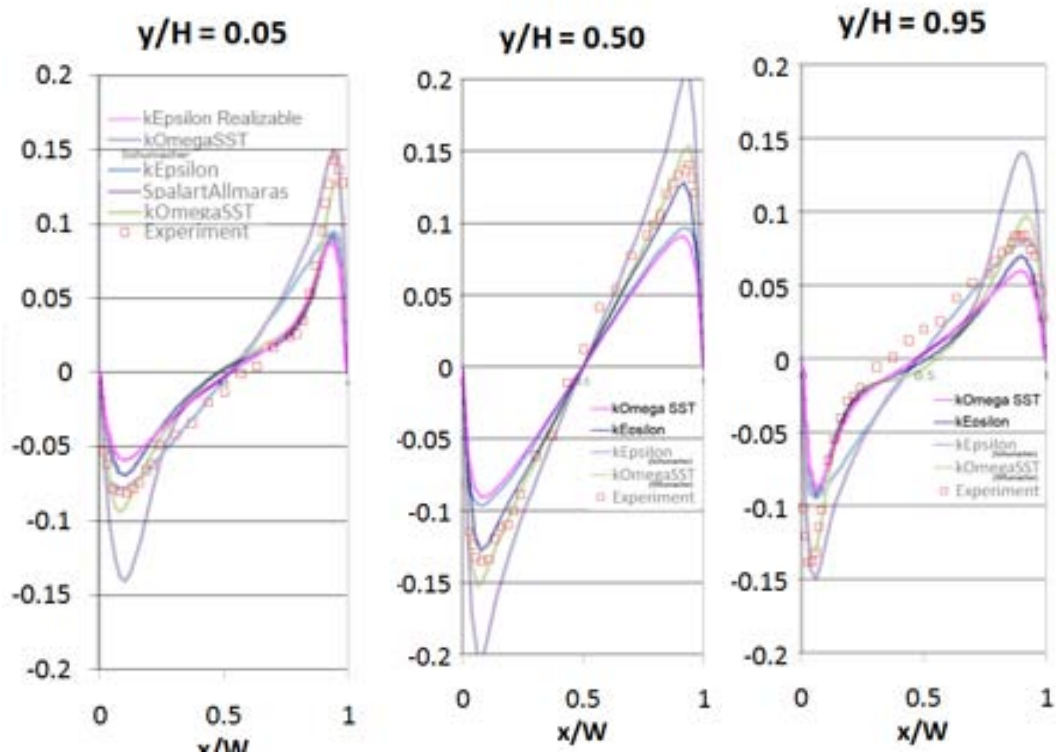
Fig. 4.2 Comparisons of Present Computations Using the k-ω SST and k-ε Realizable Vertical Velocity Profiles with Experimental Data of [Betts and Bokhari 2000 (2)] and the Computations of [de Villiers 2010 (8)]
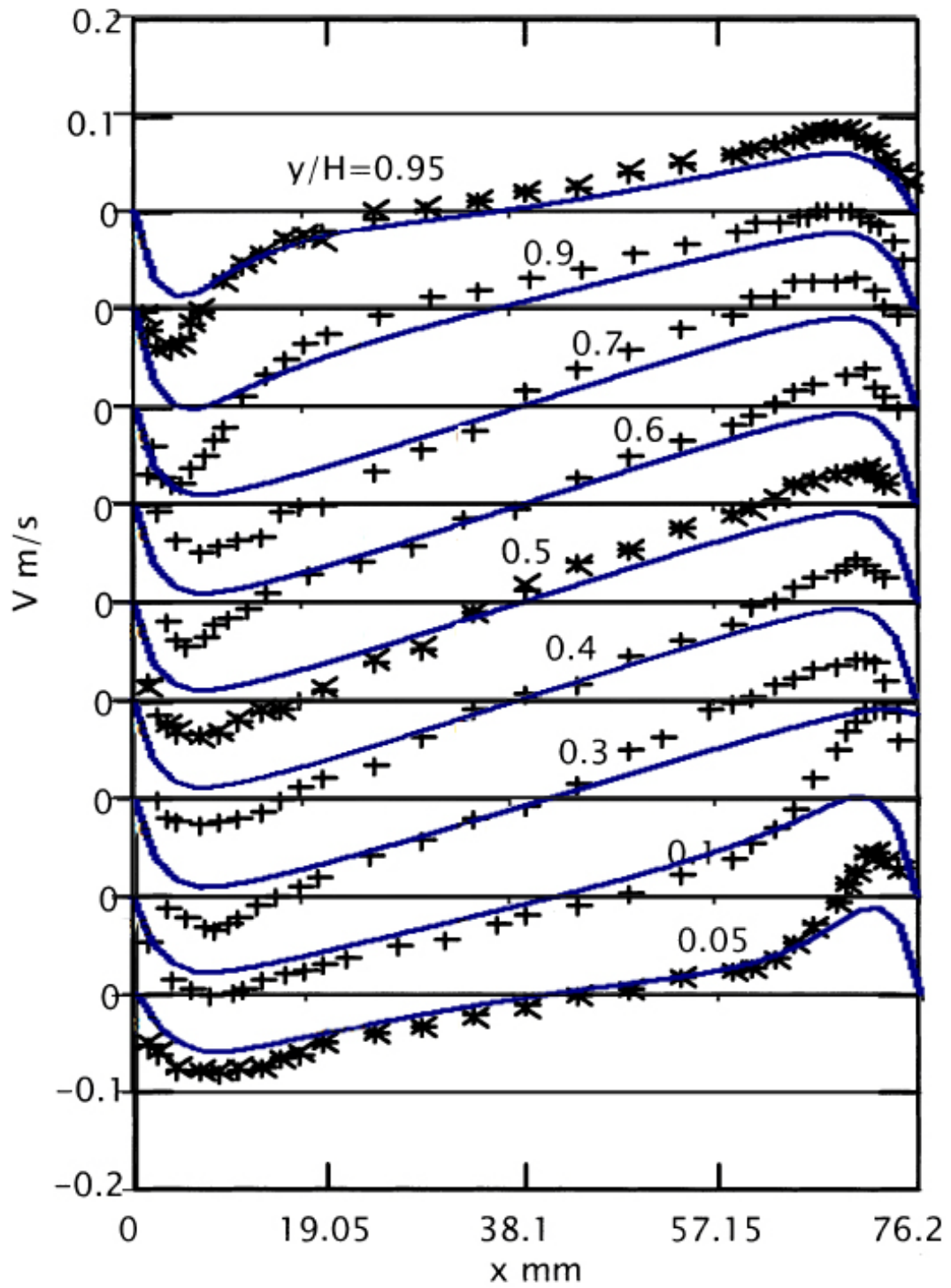
Fig. 4.3 Comparison of Present Computations for Velocity Profiles at Various y/H With the Experiments of [Betts and Bokhari 2000 (2)] Using the k-ε Realizable Model

Fig. 4.3 Comparison of Present Computations for Velocity Profiles at Various y/H With the Experiments of [Betts and Bokhari 2000 (2)] Using the k-ω SST Model

27
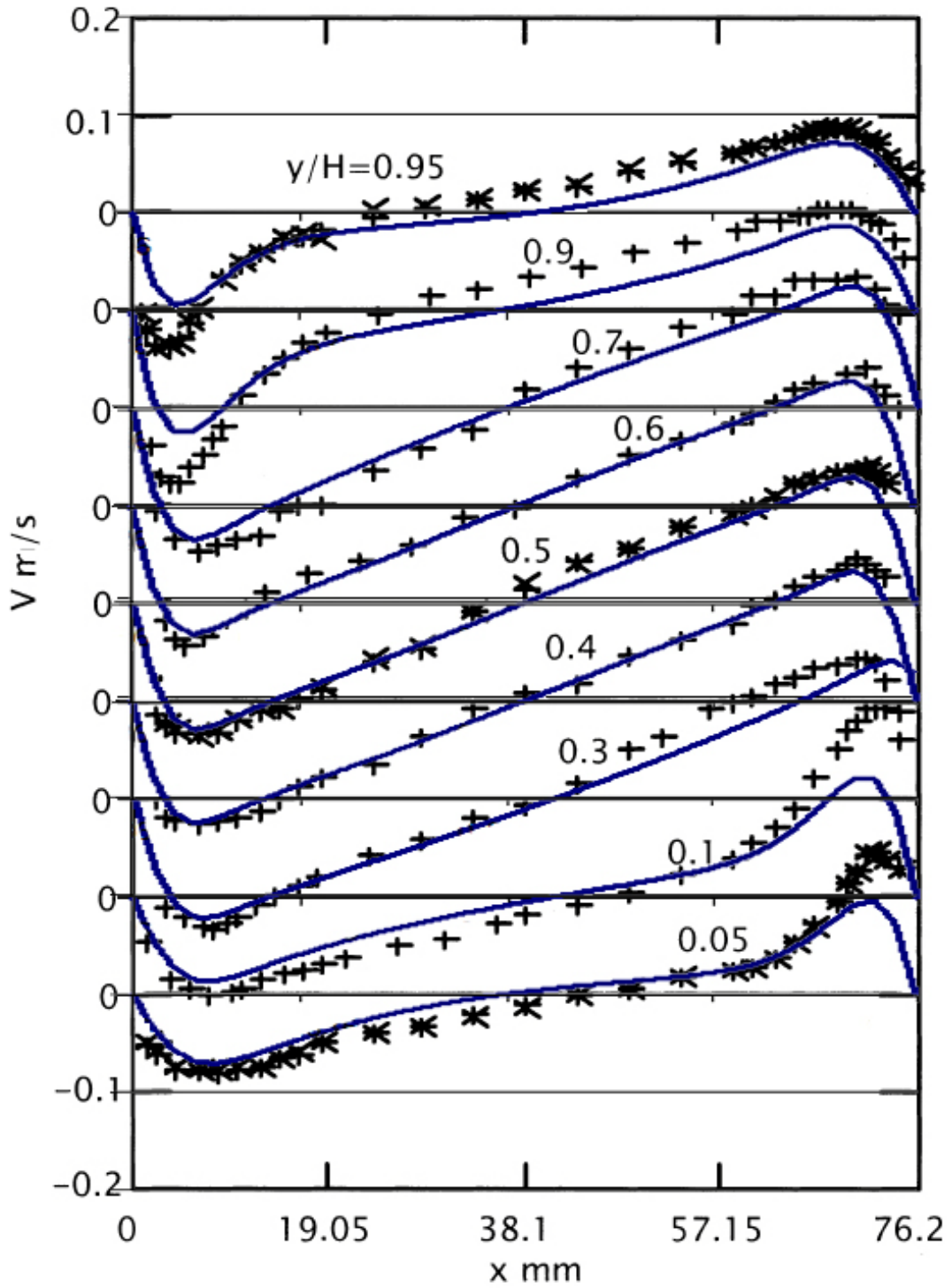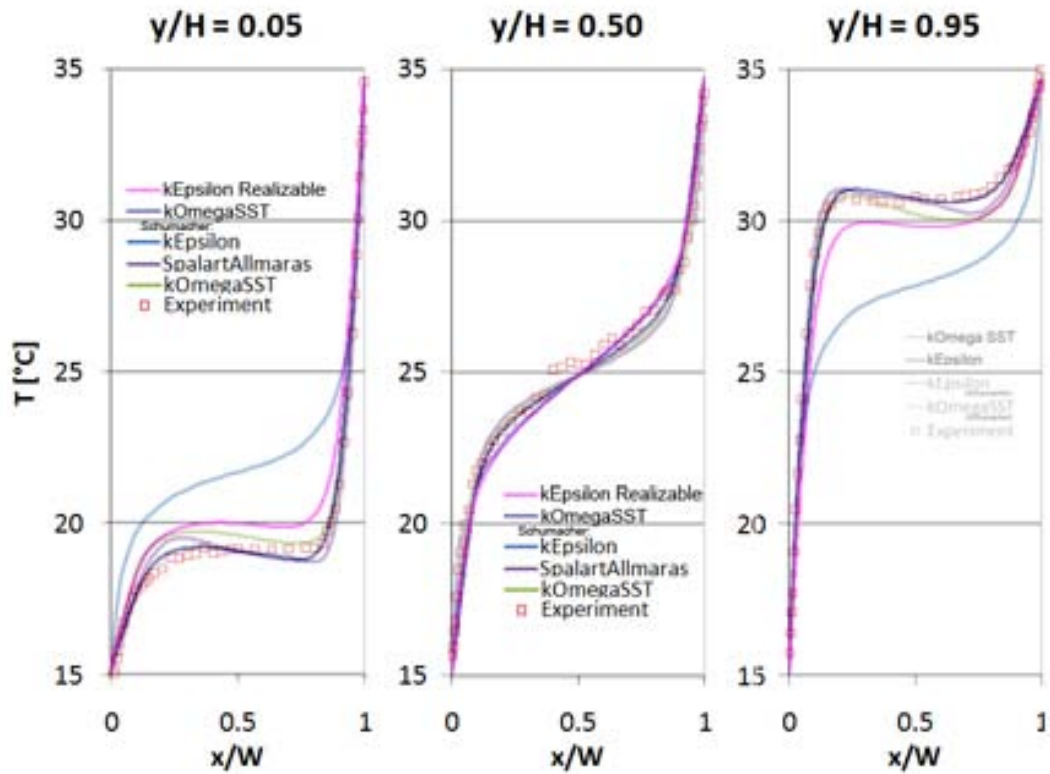
Fig. 4.5 Comparisons of Present Computations Using the k-ω SST and k-ε Realizable Temperature Profiles with Experimental Data of [Betts and Bokhari 2000 (2)] and the Computations of [de Villiers 2010 (8)]
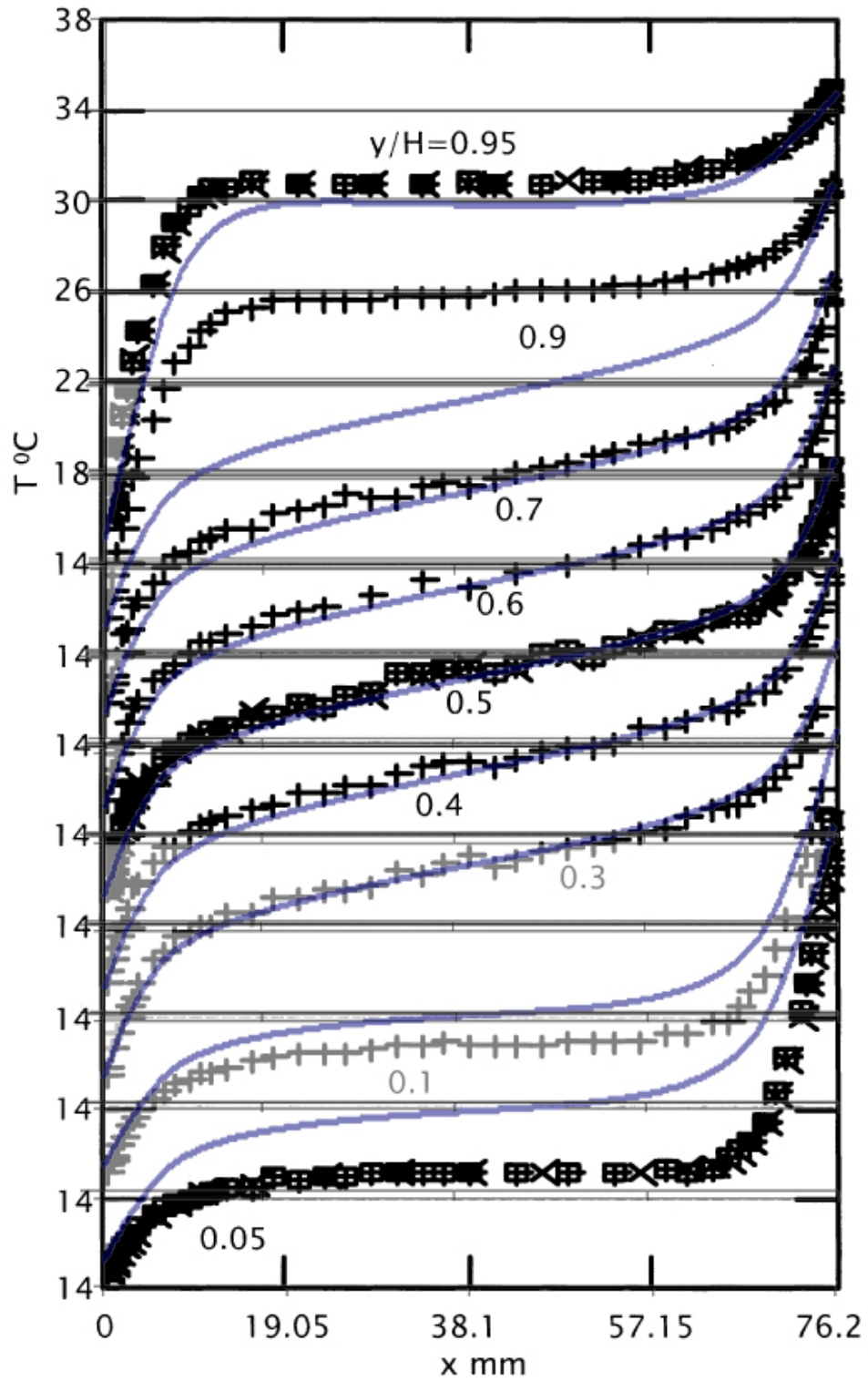
Fig. 4.6 Comparison of Present Computations for Temperature Profiles at Various y/H With the Experiments of [Betts and Bokhari 2000 (2)] Using the *k-ε* Realizable Model

29
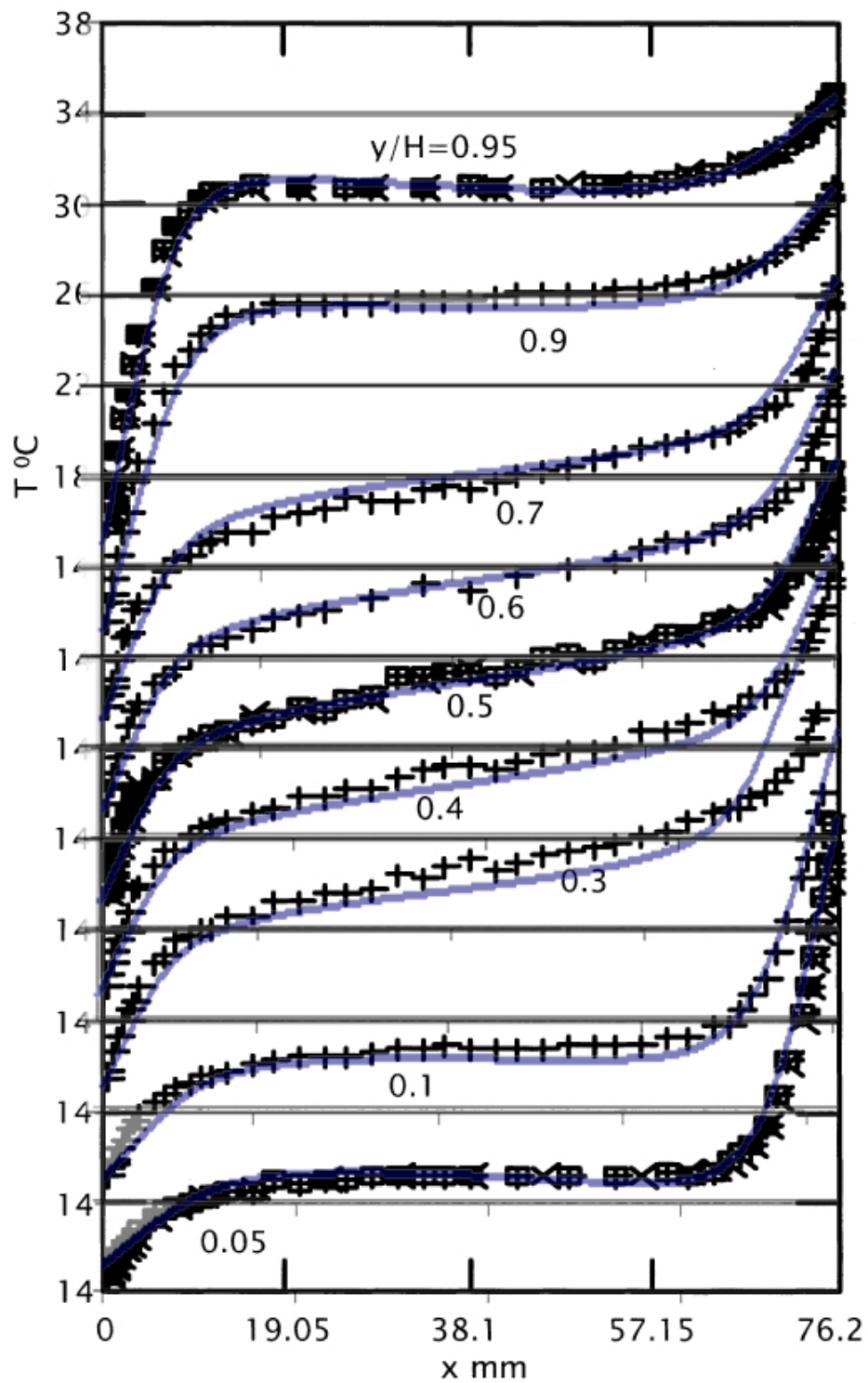
Fig. 4.7 Comparison of Present Computations for Velocity Profiles at Various y/H With the Experiments of [Betts and Bokhari 2000 (2)] Using the k-ω SST Model

Chapter 5

Simulation of Mixed Convection in a 2-D Square Cavity

5.1 2-D Model

This case is based on the experimental study of Blay et al (1992). In this case (Fig. 5.1), air is forced into a 1.04-m square cavity through an inlet of length $h = 0.018$ m on the chamber's ceiling. Like the forced convection case of Chapter 3, the air creates circulation within the chamber, and comes out through an outlet of length $t = 0.024$ m near the floor. Also, like the natural convection case of Chapter 4, the walls ceiling and floor are kept at different temperatures. The temperature of the sides, walls and ceiling is fixed at $T_{wl} = 288.15$ K, while the floor is kept at $T_{wh} = 308.65$ K. As a result, the air in the cavity is subjected to both a mixture of inertial and buoyancy forces. This case therefore represents mixed convection.
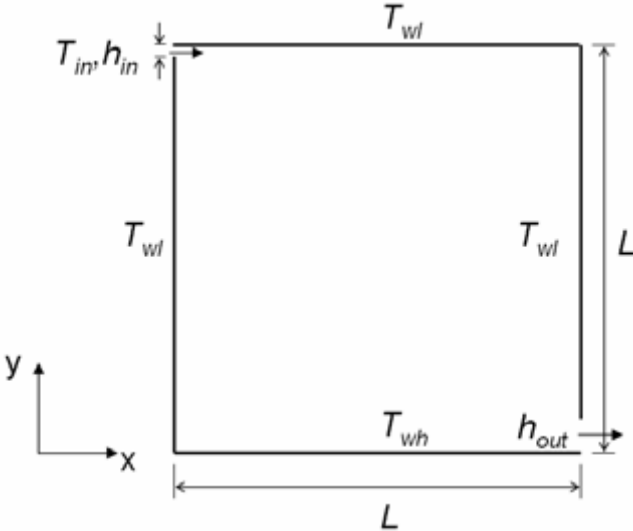
Fig. 5.1 Sketch of the Mixed Convection Model [Zuo and Chen 2009(20)]

The key goal of this study is again to validate the CFD solver for computing mixed convection flow, and to determine the relative accuracy of k-ε realizable and k-ω SST models.

5.2 Results and Discussion

Figures 5.2 and 5.3 respectively show the vertical temperature profile in the middle of the cavity and the horizontal temperature profile in the middle of the cavity. In this case, present computations with the k-ε realizable model are in closer agreement with the experimental data, although the k-ω SST model also gives acceptable results. The computational results of de Villiers (2010) show a greater disagreement with the experimental data.
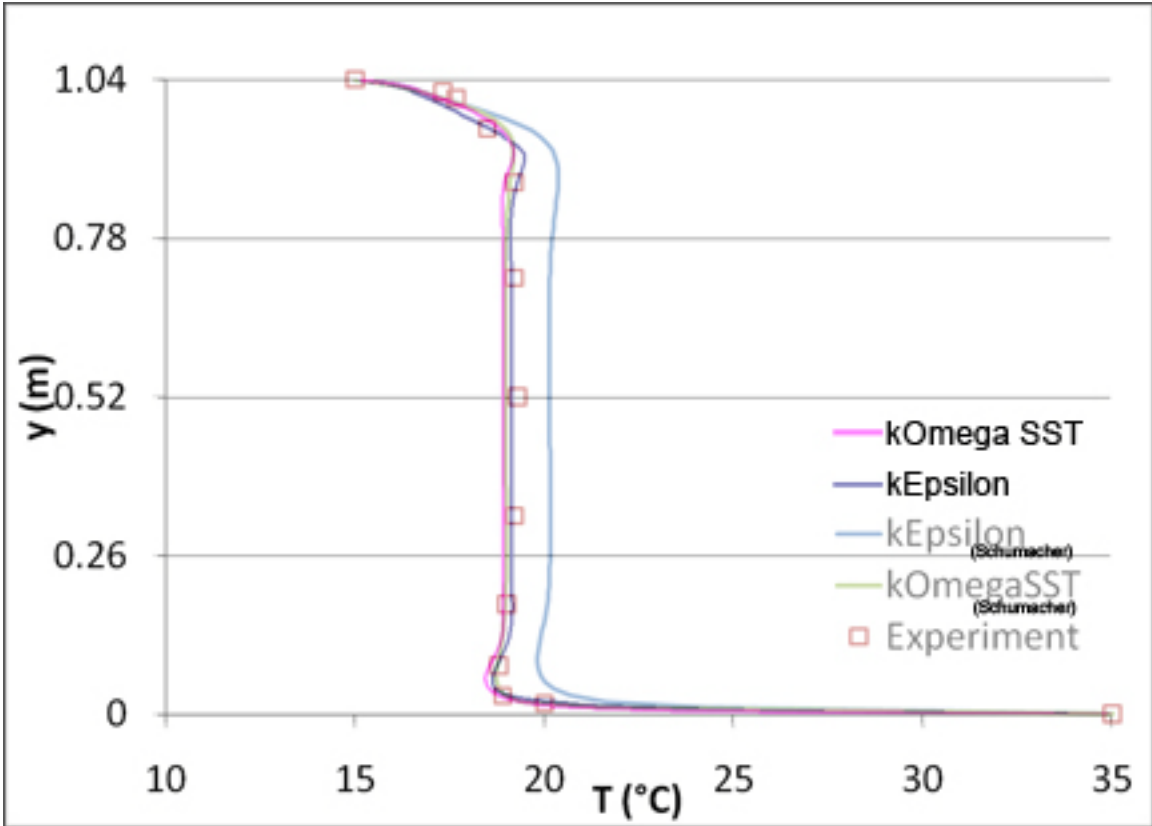
Fig. 5.2 Comparison of Present Computations With k-ε Realizable and k-w SST Models for the Temperature Profile at x = L/2, With Experimental Data [Blay et al. 1992 (3)] and the Computations of [De Villiers 2010 (8)]
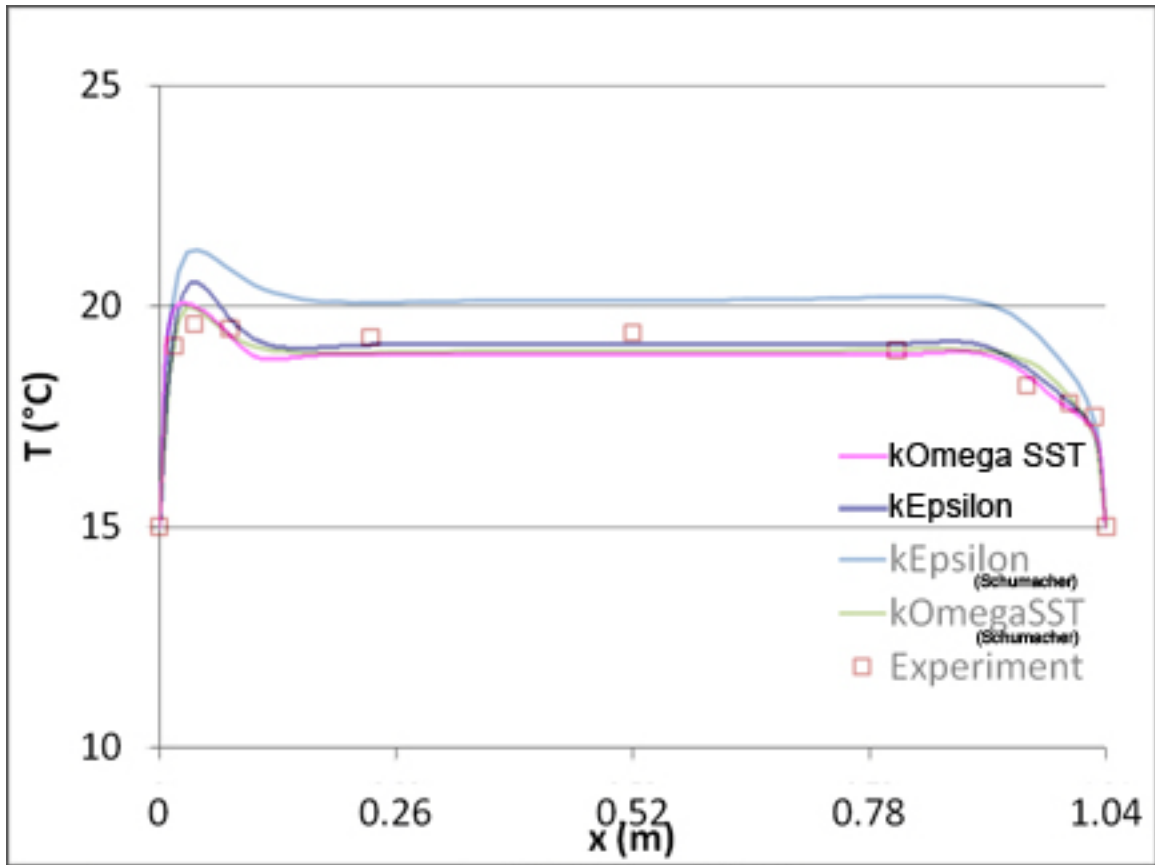
Fig. 5.2 Comparison of Present Computations With *k-ε* Realizable and k-w SST Models for the Temperature Profile at y = L/2, With Experimental Data [Blay et al. 1992 (3)] and the Computations of [De Villiers 2010 (8)]

Figures 5.4 and 5.5 show the comparison of experimental velocity contours (shown by arrows) with those computed by Zuo and Chen (2009) using the *k-ε* realizable and *k-ω* SST turbulence models, respectively. It can be seen that the flow field velocity contours computed with the *k-ω* SST model are in better agreement with the experimental data.
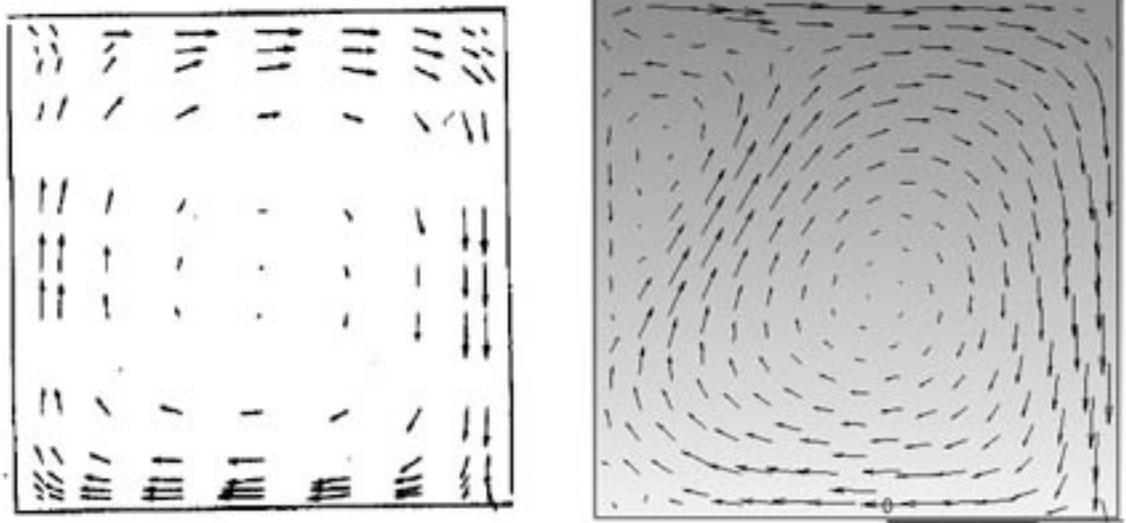
Fig. 5.4 Comparison of Experimental Velocity Contours (left) with Present Computed Velocity Contours using the *k-ε* Realizable Model [Zuo and Chen 2009 (20)]
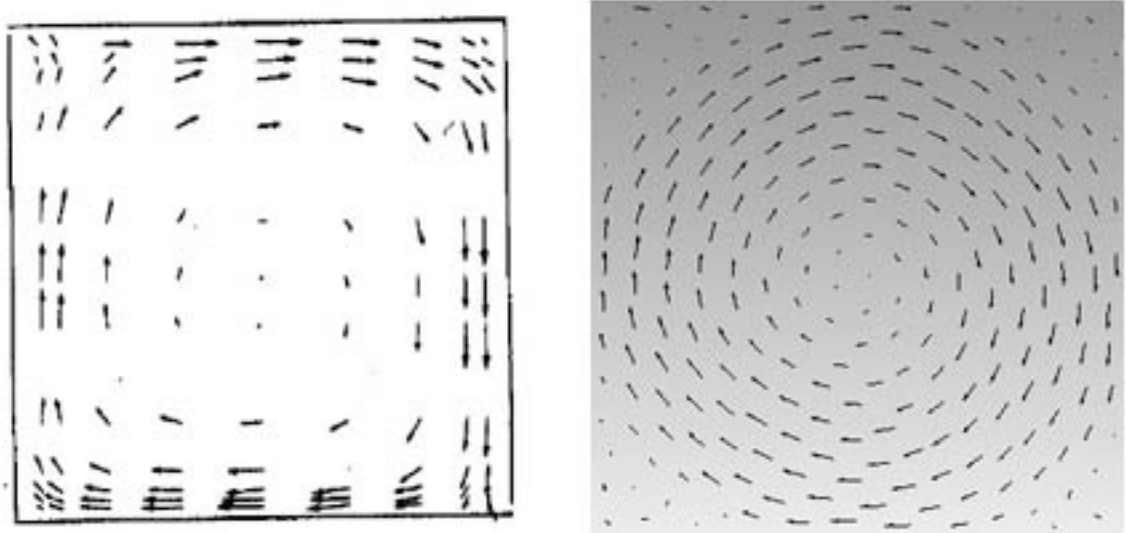
Fig. 5.5 Comparison of Experimental Velocity Contours (left) with Present Computed Velocity Contours using the *k-ω* SST Model [Zuo and Chen 2009 (20)]

Figures 5.5 and 5.6 show the computed temperature contours using the *k-ε* realizable and *k-ω* SST turbulence models, respectively. These contours indicate that the *k-ε* realizable model is more accurate near the walls, while the *k-ω* SST model is more accurate in the middle region of the cavity.

34
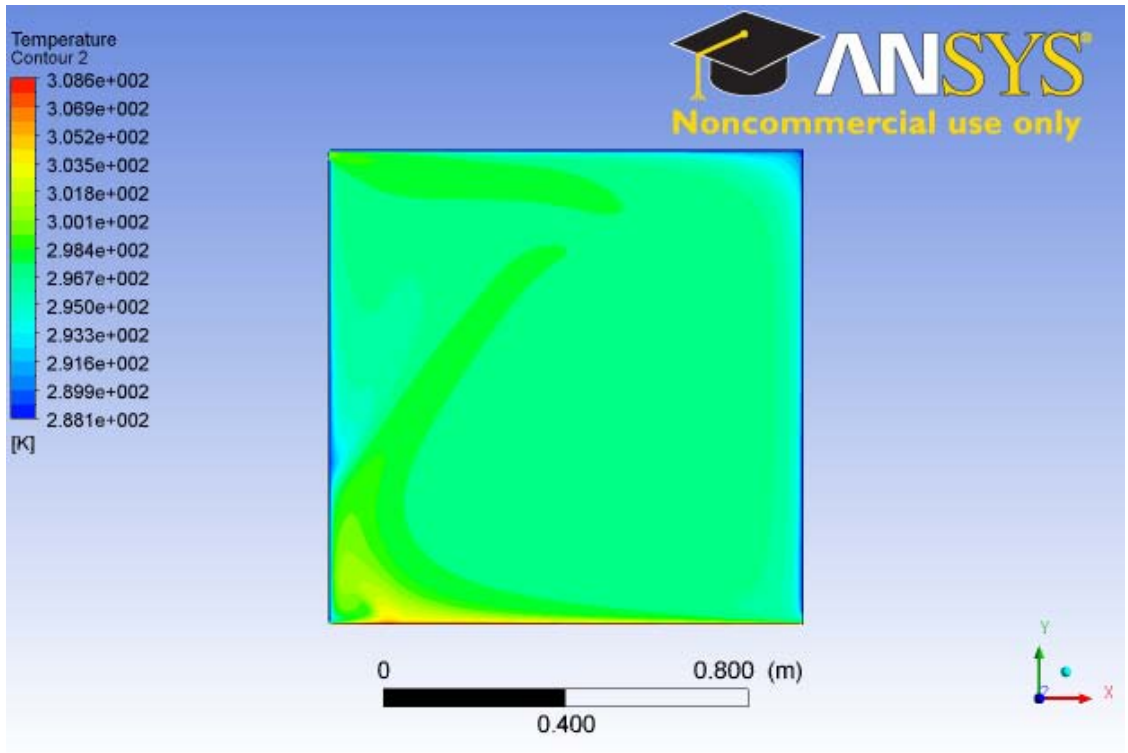
Fig. 5.6 Computed Temperature Contours Obtained With the k-ε Realizable Model
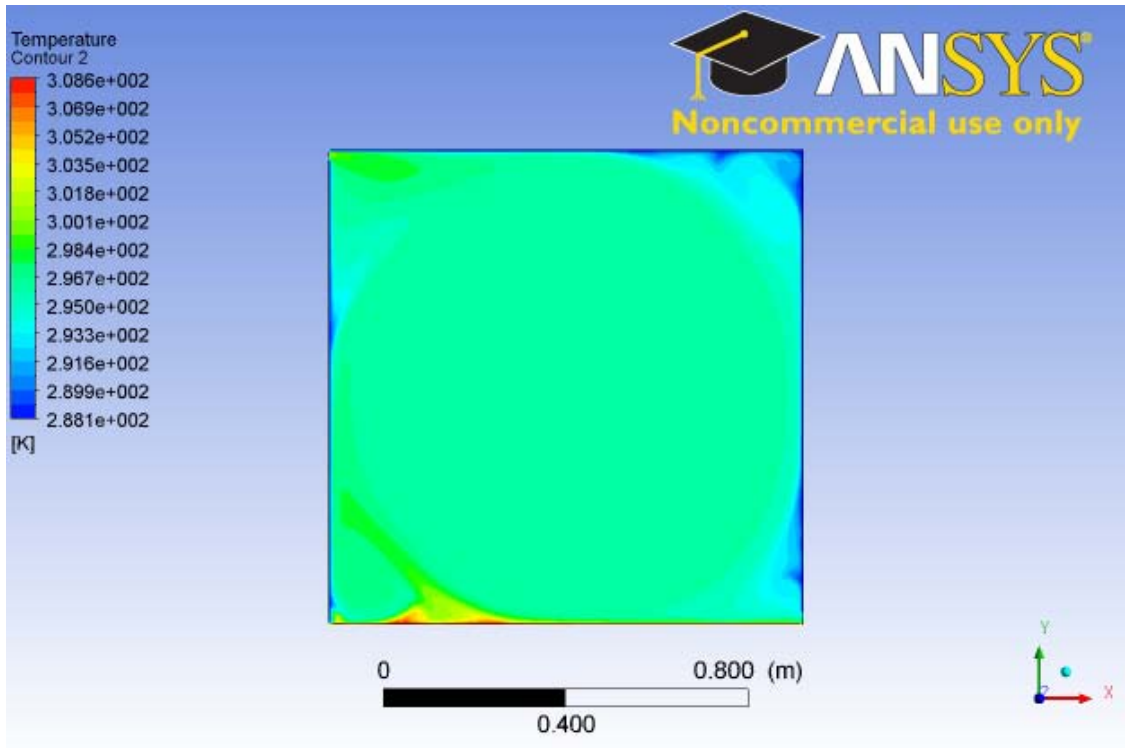
Fig. 5.7 Computed Temperature Contours Obtained With the k-ω SST Model

Chapter 6

Modeling Air Flow in a 3-D Enclosure Under Natural Ventilation

6.1 3-D Model

This model is based on the experimental study of Jiang and Chen (2003) to simulate the indoor environment of a 3-D chamber with a single outlet. In the study, a 5.16 x 3.57 x 2.18 m^3 room was supplied with a single 1,500 W baseboard heater to generate buoyancy forces. In addition, a 0.9 x 1.80 m^2 opening was constructed in the opposite wall to simulate fluid flow between the room and a "windless" outdoor environment, thereby creating a single-sided ventilation driven by buoyancy forces. Figure 6.1 shows the two views describing the floor plan of the room.
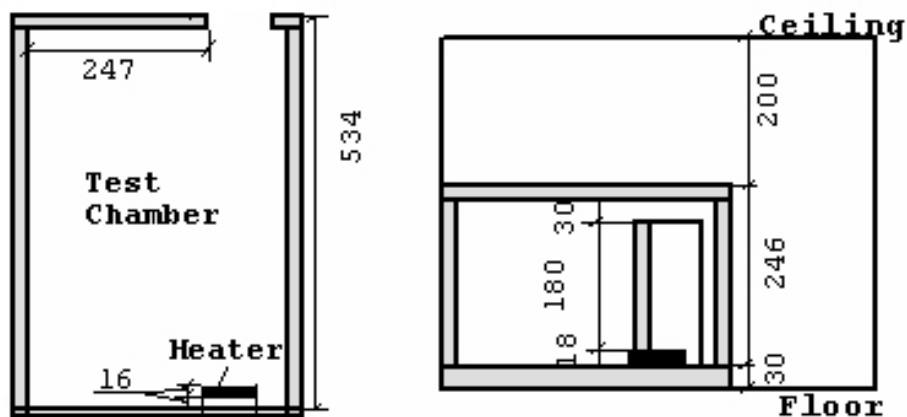
Fig. 6.1 Floor Plan of the 3-D Natural Convection Experiment [Jiang and Chen 2003 (12)]
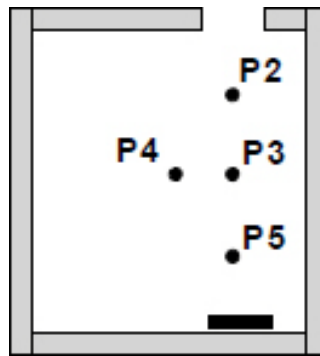
Fig. 6.2 Location of Temperature and Velocity Probe Positions In the Vertical Cross-Section [Jiang and Chen 2003 (12)]

In this study, "air velocity and temperature distributions were measured with six hot-sphere anemometers at different heights (0.1 m, 0.5 m, 0.9 m, 1.3 m, 1.7 m, and 2.1 m from the floor) in five different locations" (Jiang and Chan 2003) as shown in Figure 6.2. These devices displayed considerable uncertainty at air velocities of less than 0.1 m/s; temperature measurement error was 3 K. In addition, since the goal of the study was "to examine the overall airflow pattern in a room scale driven by buoyancy forces" (Jiang 2012), the heater's surface temperature and micro-scale thermal environment was not measured. Figure 6.3 shows the 3-D sketch of the room used in the computational study.
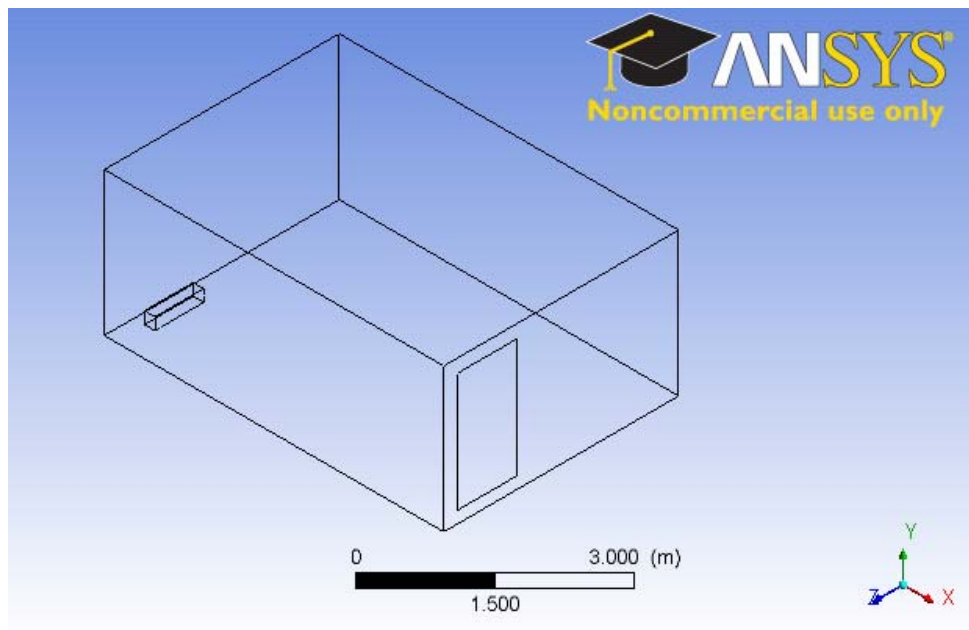
Fig. 6.3 Sketch of the 3-D Natural Convection Model

37

In the absence of the availability of detailed data from the experiment, several assumptions were made in the computations regarding the wall, heater and air temperatures. While the heater was modeled with the same dimensions (0.16 m x 0.74 m x 0.18 m) as stated in the experimental study, the temperature along all five exposed walls was assumed to be 350 K. The surrounding walls were assumed to be adiabatic, held at 300 K, and the air characteristics were assumed to be the same as those given in Section 2.8 for the 2-D cases.. The window was assumed to be a pressure outlet with a gauge pressure of 0; the air outside the enclosure was assumed to be at 288 K. Based on our good experience with the k-ω SST model in the 2-D natural convection problem described in Chapter 4, it was chosen for this study.

4.2 Results and Discussion

Figure 6.4 shows the computed temperature contours in the room's section that contains temperature probes P2, P3 and P5. As can be seen from the contour the solution satisfies the adiabatic wall conditions in the room, with the exception of the window outlet through which air flows through freely. The contours also show that aside from the air immediately surrounding the heater, temperature remains between 288 and 300 K.

Figures 6.5 and 6.6 are the velocity vector plots in the same section that contains the P2, P3 and P5 probes. Figure 6.5 shows the velocity vector contours from the study of Jiang and Chen (2009) and Figure 6.6 shows the velocity vector contours obtained in the present computations. Both Figures 6.5 and 6.6 show qualitatively similar results inside the chamber; however, there is significant difference in the flow field near the ceiling. In both figures the air enters through the lower section of the window, moves rapidly near the floor and the wall, and circulates back along the ceiling to exit the room on the upper section of the outlet. The computation shows evidence of recirculation in the upper left corner of the room; however, unlike the Jiang and Chen results in Figure 6.5, the airstream diverges into two distinct areas: one continues the recirculation

pattern and the other moves at higher speed straight towards the ceiling. The reason for this behavior is currently under investigation.
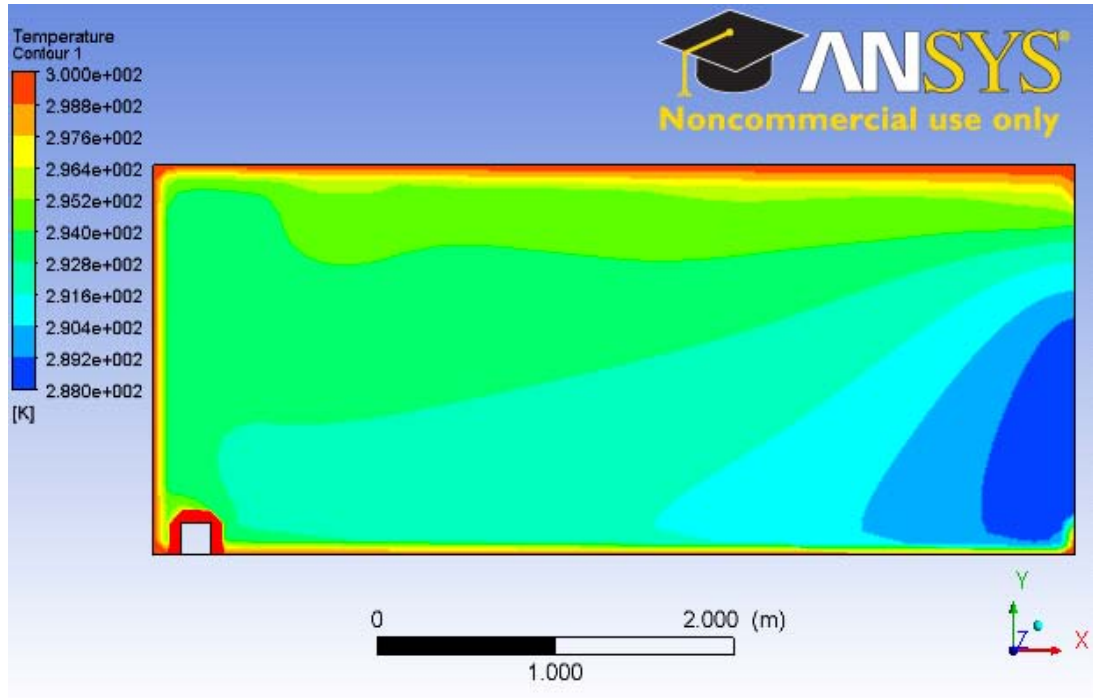
Fig. 6.4 Temperature Contours in the Room at a Section Containing Probes P2-P3-P5
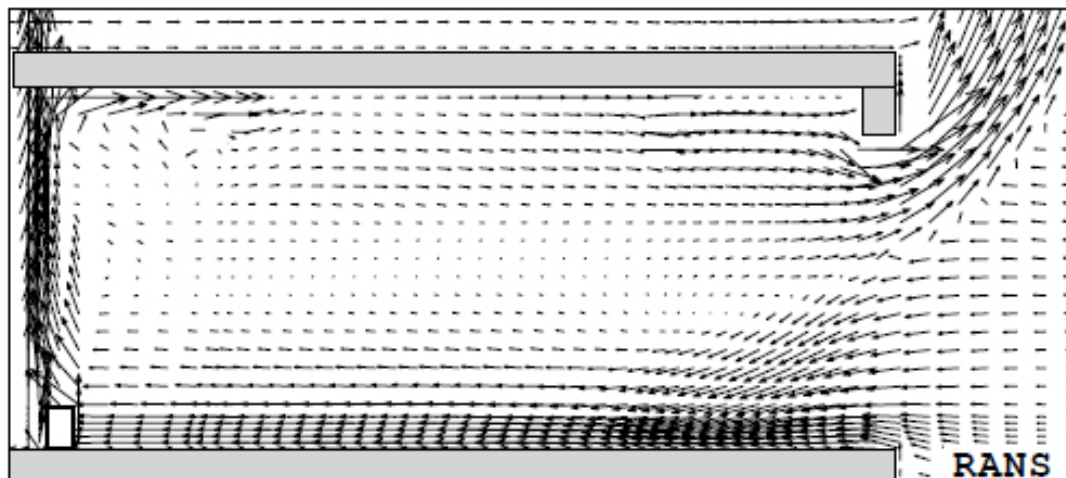
Fig. 6.5 Velocity Vector Contours Inside the Section Containing the P2, P3, and P5 Probes [Jiang and Chen 2003 (12)]
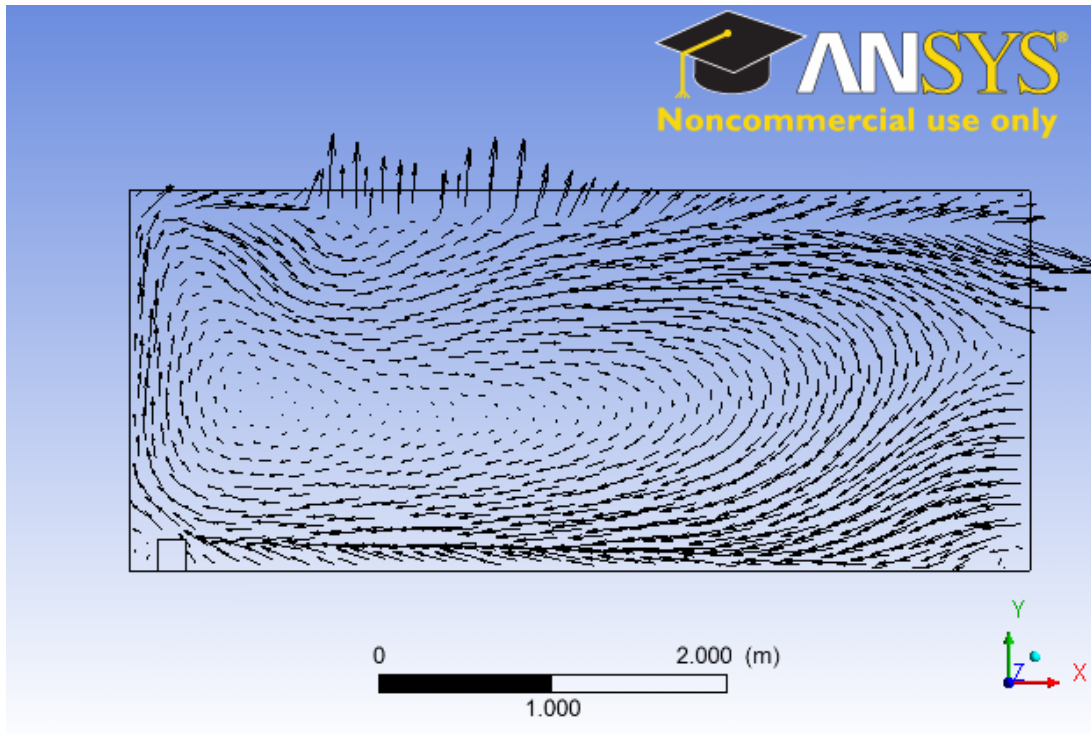
Fig. 6.6 Computed Velocity Vector Contours Using the *k-ω* SST Model Inside the Section of the Room Containing the P2, P3, P5 Probes

Figures 6.6 and 6.7 respectively show the comparisons of experimental and computed temperature and velocity profiles at four of the five probe locations. The fifth probe, being outside of the room, has been neglected. Since the computational model was created based on a number of assumptions on due to paucity of information, a direct comparison with the experimental data is not possible; therefore, a qualitative analysis is given. The experimental temperature profiles show close resemblance with their numerical counterparts. Specifically, temperatures remain low near the floor and increase with height. Velocity profiles also show similar results, indicating a period of stagnation near the center of the room which is surrounded by the circulating air. Qualitatively, the experimental and computational results show similar trends in velocity and temperature profiles.
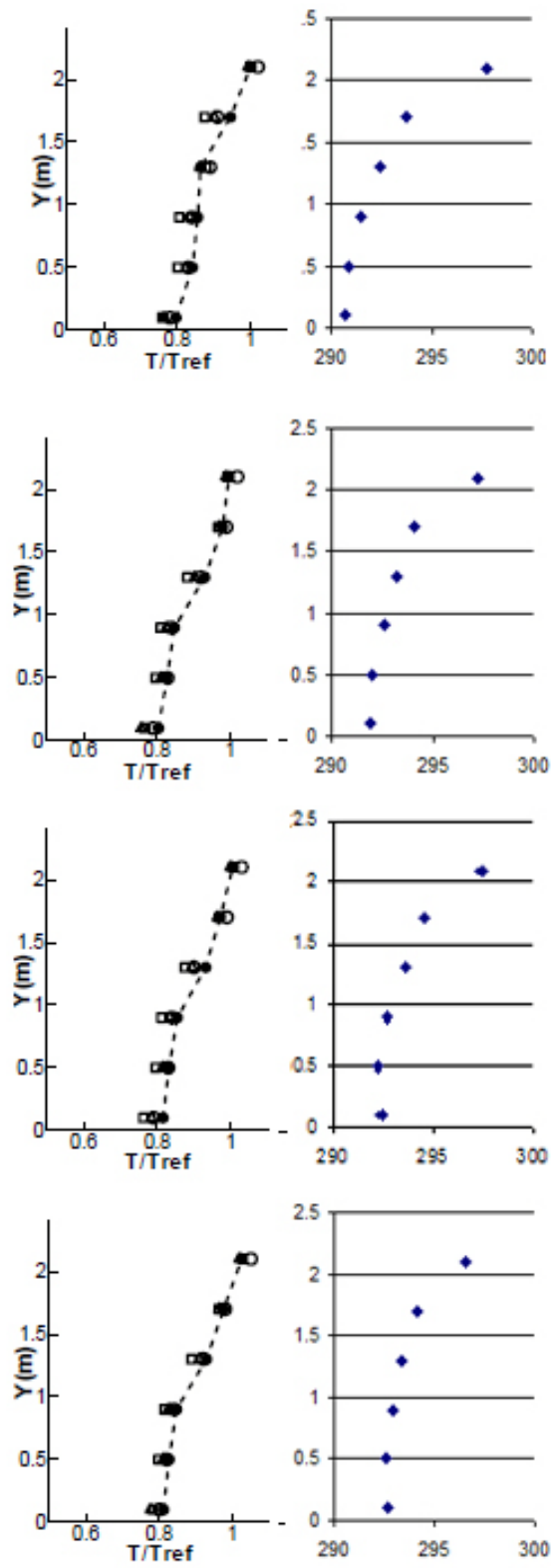
Fig. 6.7 Comparison of Experimental (Left) and Numerical (Right) Results for Mean Air Temperature Profiles at P2, P3, P4, and P5 Locations [Jiang and Chen 2003 (12)]

41
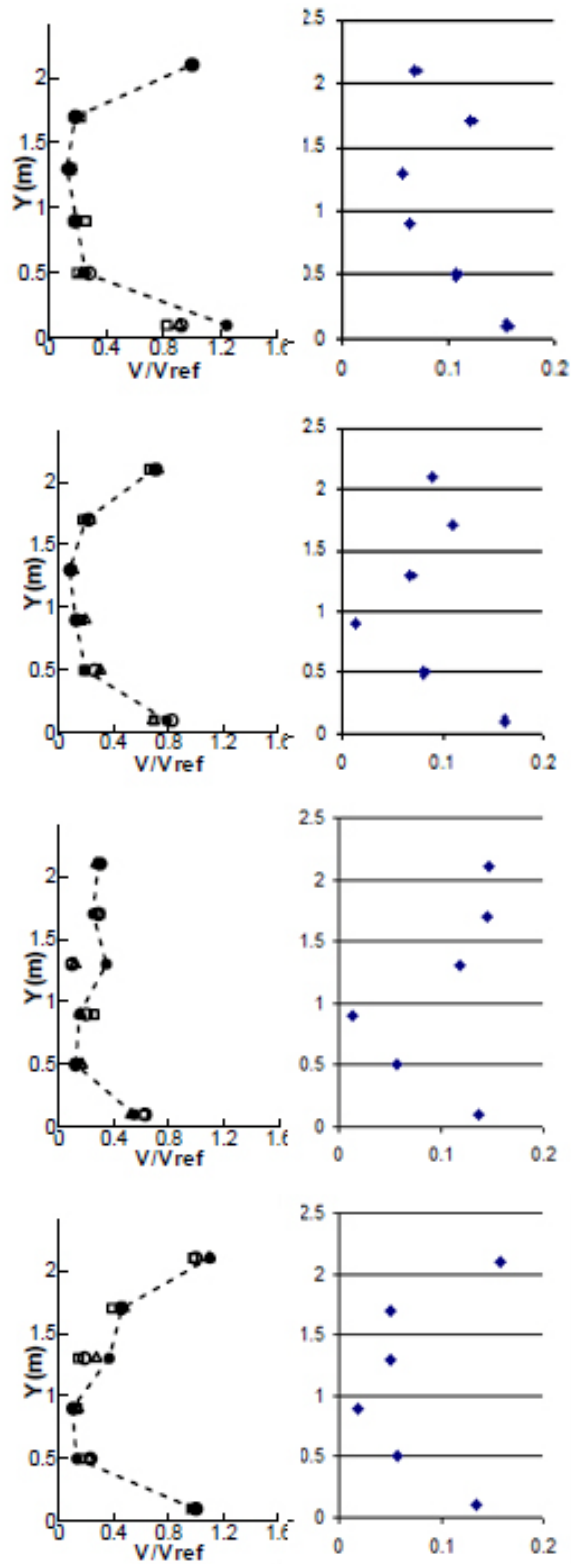
Fig. 6.8 Comparison of Experimental (Left) and Numerical (Right) Results for Mean Air Velocity Profiles at P2, P3, P4, and P5 Locations [Jiang and Chen 2003 (12)]

42

Chapter 7

Modeling of Air Flow in a 3-D Atrium Under Forced Convection and Solar Radiation

7.1 3-D Model

This test case is based on the experiments performed by Basarir (2009) in the atrium of Concordia University's Engineering building (Figs. 7.1-7.3). The atrium's size is 12.05 m x 9.39 m x 13.02 m, and it contains both a supply and return vent on its east wall. The supply vent forces air at a temperature of 288 K into the room at a speed of 4.5 m/s; the Reynolds number is 146633 based on the floor conditions at the supply vent. The Reynolds number indicates that the flow is turbulent.

The atrium's main feature is an argon-filled double-glazed glass façade that covers the entire south wall. This glass façade has a transmittance of 36%, an absorptivity of 17.5%, a thermal conductivity of 0.0626 W/m-K and thickness of 24 mm. Noting variables such as wind speed and clear weather, the effective sky temperature was calculated to be 14.21° C, and the solar direction vector was calculated to be (-0.60, 0.69, -0.40) at the time of the experiment (Basarir 2009).

Our goal is to create a CFD model that could reproduce the experimental results; in particular, the temperature profile of the building at 4:00 PM on August 1, 2007 (Basarir 2009). The mesh inside the atrium model was constructed using a mesh of 0.125 m. This generated a mesh with 844584 nodes, necessitating a computationally intensive simulation. To reduce the computational time, the convergence criteria were reduced to 1×10^{-4}. The k-ε realizable turbulence model was chosen for this case since it had proven to be more accurate in both the 2-D Forced- and Mixed Convection cases described in Chapters 3 and 5 respectively. The Discrete Transfer Radiation Model was

activated in FLUENT to track the effects due to solar radiation. It is important to note here that the glass façade cannot be opaque because it transmits the solar radiation inside the atrium. Therefore its material properties should be carefully taken into account in the CFD model.
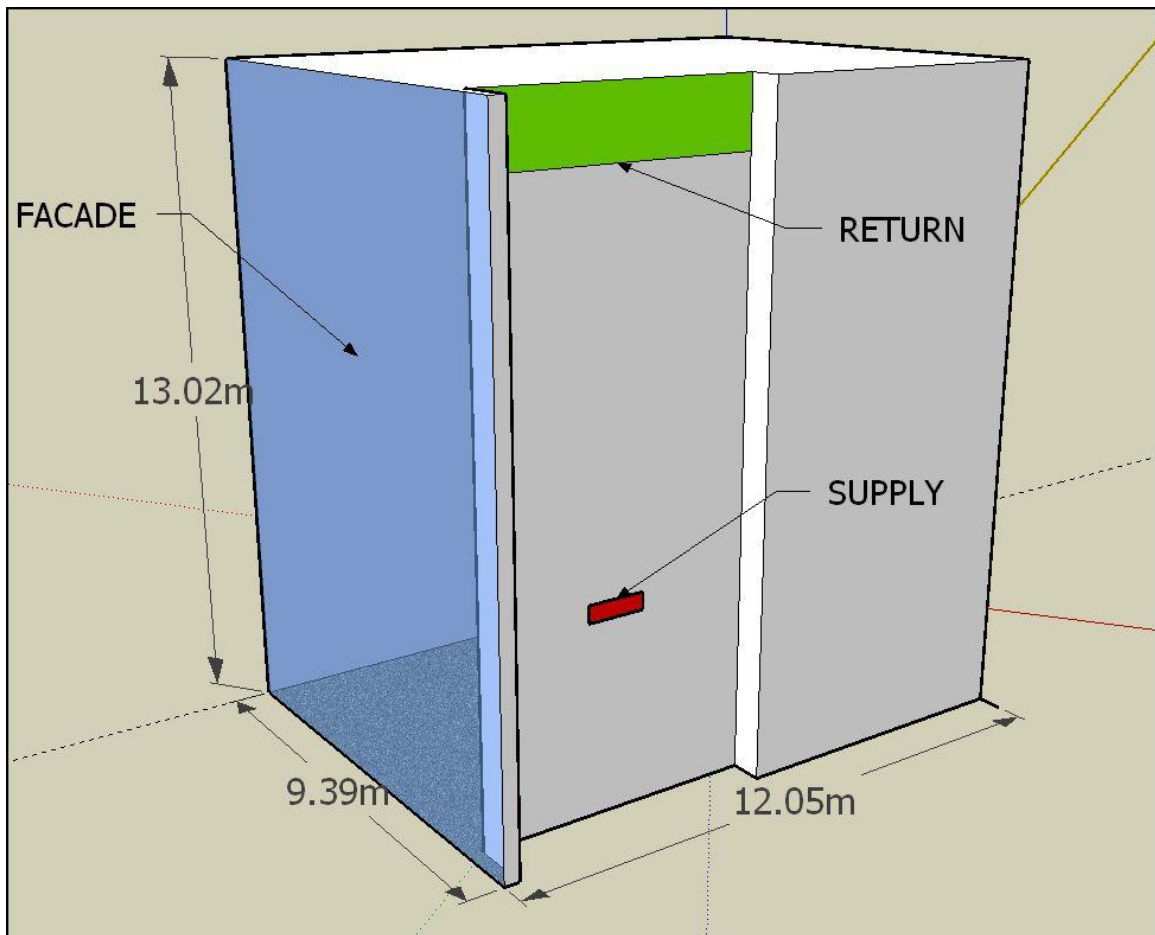
Fig. 7.1 Concordia University's Engineering Building Atrium [Basarir 2009 (1)]
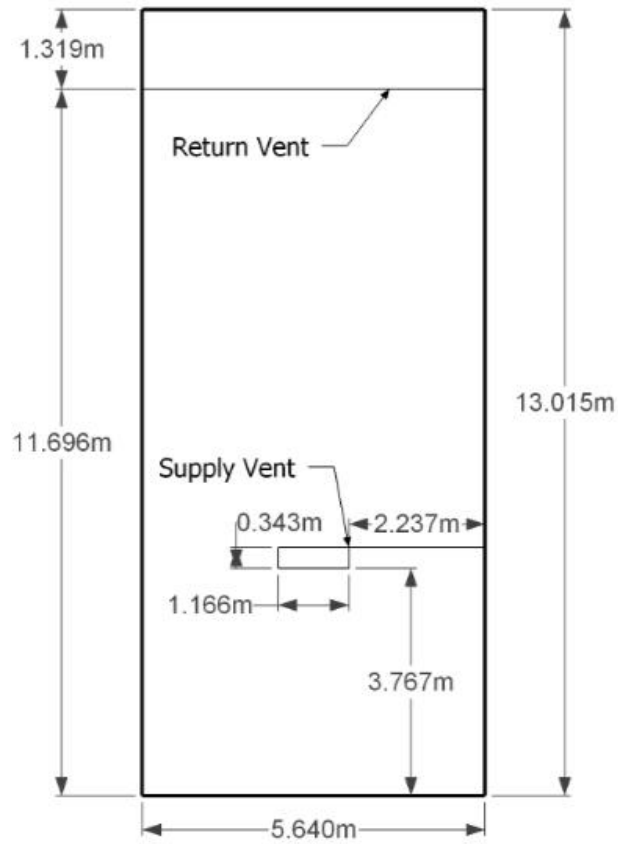
Fig. 7.2 Dimensions of the Supply and Return Vents on the East Wall of the Atrium [Basarir 2009 (1)]
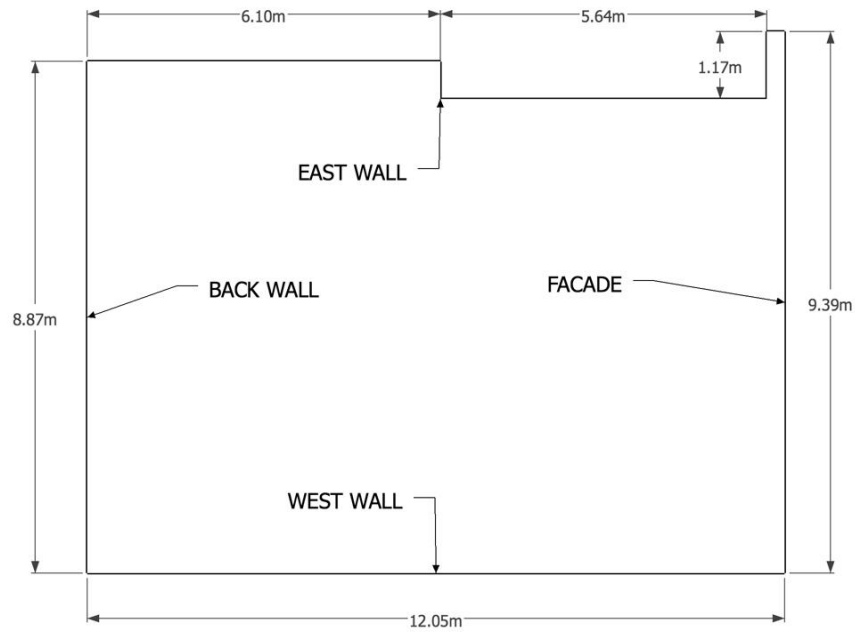
Fig. 7.3 Floor Plan of the Atrium [Basarir 2009 (1)]

45

7.2 Results and Discussion

Figures 7.4 and 7.5 show the temperature contours on the building's façade from the Basarir (2009) experimental study and the present computational study using the k-ε model. It can be noted that from both the figures that the left side of the façade is considerably warmer than the rest of the façade. This means that the left side of the atrium will be warmer than the rest of the atrium due to "a wall that partially traps the hot air." Furthermore, the lower right side has a considerable accumulation of cold air near the right wall, possibly due to the "impingement of the cool supply air on this wall." There is also evidence of circulation in both of the figures, particularly in the lower middle of the room. It should be noted, however, that on the whole, the computational results computed with the k-ε model is show lower temperatures than Basarir's experiments.

Figures 7.6 and 7.7 show the contour plots of the numerically predicted temperatures by Basarir (2009) and the writer of this thesis at heights of 2, 6.165 and 10.25 meters above the floor. Once again it can be noticed that, there is a considerable accumulation of cold air on the lower end of the west wall, and the effects of the trapped air on the east end of the façade have become more pronounced. Especially noteworthy are the low-temperature contours running parallel to the façade in the y=2 plane. These contour plots, and the fact that they are below the supply vent, lends credence to Basarir's claim that the circulation is responsible for the cool air against the east wall. Again, the temperature distribution obtained with the k-ε realizable model is cooler than those obtained by Basarir (2009).
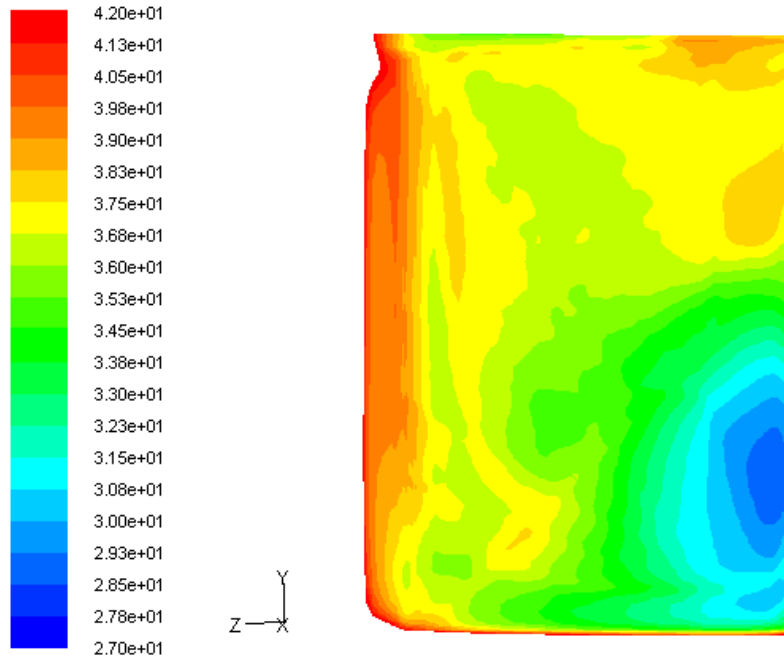
Fig. 7.4 Temperature Contours on the Glass Façade In Basarir's Experiment [2009 (1)]
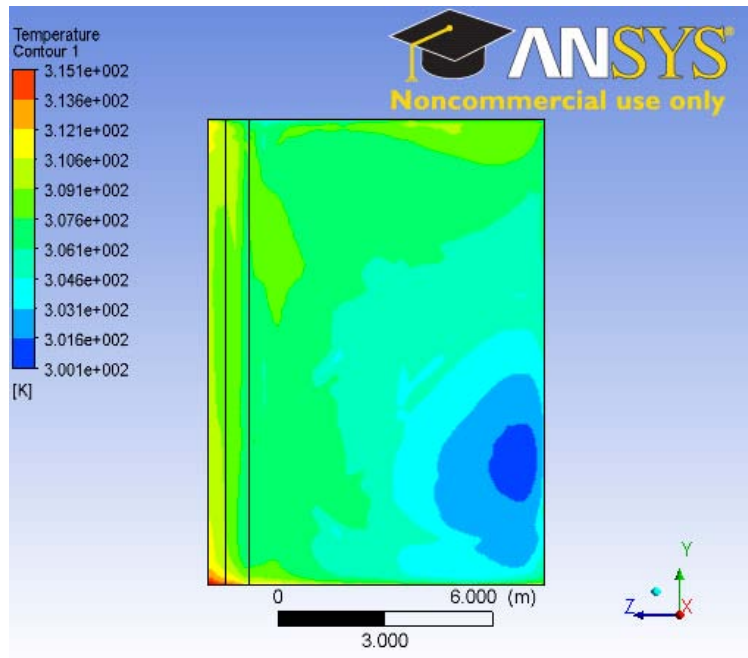
Fig. 7.5 Computed Temperature Contours on the Glass Façade Using the *k-ε* Realizable Turbulence model
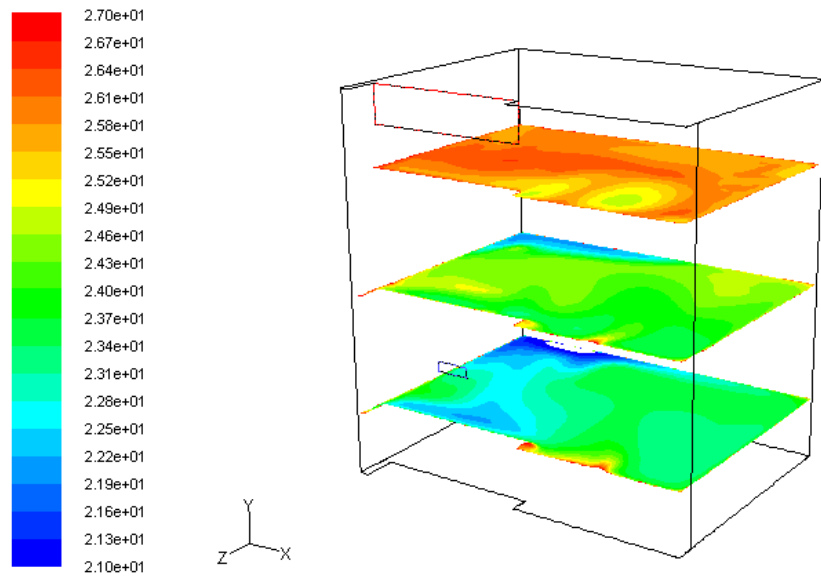
Fig. 7.6 Temperature Contours in the Atrium of y=2, y=6.165 and y=10.25 Planes in Basarir's Computations [2009 (1)]
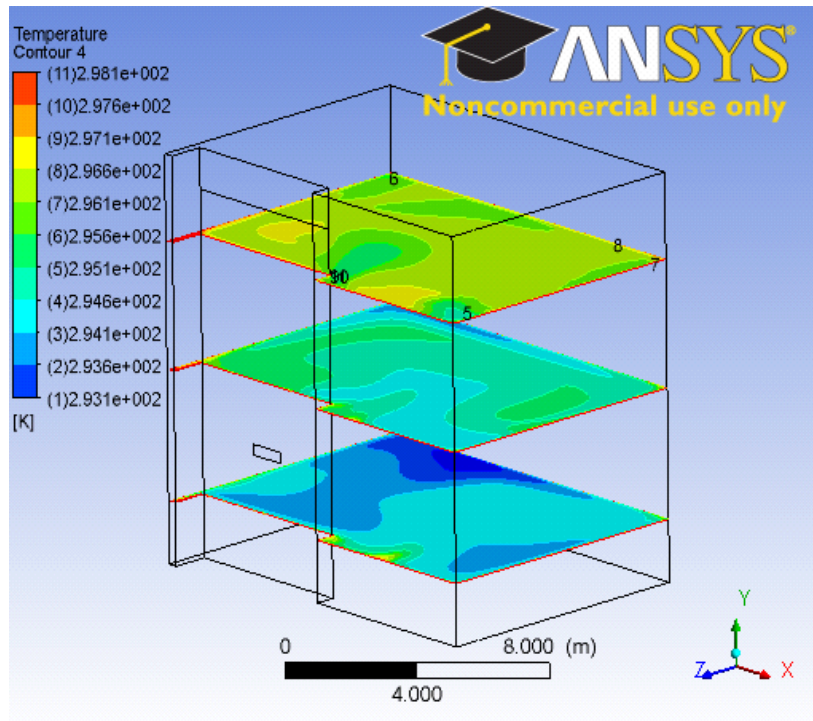
Fig. 7.7 Temperature Contours in the Atrium at y=2, y=6.165 and y=10.25 Planes in the Present Computations Using the *k*-ɛ Realizable Turbulence Model

Experimental data for this study was collected via a network of 12 thermocouples on the glass façade and 21 additional thermocouples distributed in the interior space of the atrium. As a result, it is possible to compare experimental data with numerical results in greater detail as shown in Tables 1 and 2. As can be seen from the tables, the k-ε model yields very accurate results for the façade, particularly on the upper level of the building where deviation from experimental results is ~-0.5%. The same could not be said of the air temperature results, as they are consistently 12-15% lower than the experimental data.

GLASS HIGH	Coordinates	Temperature T (°C) Experimental	Numerical	ΔT (°C)	Percent Difference
FL_G_T	0,10.25,7.26	34.20	34.66	0.46	1.3%
FM_G_TH	0,10.9,4.22	34.90	33.80	-1.10	-3.2%
FM_G_TL	0.9.35,4.22	33.60	33.47	-0.13	-0.4%
FR_G_T	1,10.25,1.24	32.80	32.93	0.13	0.4%
Average		33.88	33.72	-0.16	-0.5%

GLASS HIGH	Coordinates	Temperature T (°C) Experimental	Numerical	ΔT (°C)	Percent Difference
FL_G_M	0,6.165,7.26	31.70	34.19	2.49	7.8%
FM_G_MH	0,6.9,4.22	34.10	32.00	-2.10	-6.1%
FM_G_ML	0,5.2,4.22	31.70	31.56	-0.14	-0.5%
FR_G_M	0,6.165,1.24	32.50	30.45	-2.05	-6.3%
Average		32.50	32.05	-0.45	-1.4%

GLASS HIGH	Coordinates	Temperature T (°C) Experimental	Numerical	ΔT (°C)	Percent Difference
FL_G_B	0,2.1,7.26	30.90	33.33	2.43	7.9%
FM_G_BH	0,3.05,4.22	30.10	31.41	1.31	4.3%
FM_G_BL	0,1.35,4.22	29.50	32.63	3.13	10.6%
FR_G_B	0,2.1,1.24	29.80	28.76	-1.04	-3.5%
Average		30.08	31.53	1.46	4.9%

Table 1: Temperatures on the Glass Façade: Comparison Between Experimental [Basarir 2009 (1)] and Present Numerical Data

AIR HIGH	Coordinates	Temperature T (°C)		ΔT (°C)	Percent Difference
		Experimental	Numerical		
FL_R_T	0.24,10.25,7.26	26.80	23.55	-3.25	-12.1%
FM_R_TH	0.24,10.9,4.22	28.20	23.44	-4.76	**-16.9%**
FM_R_TL	0.24,9.35,4.22	27.20	22.86	-4.34	**-15.9%**
FR_R_T	0.24,10.25,1.24	26.60	24.00	-2.60	-9.8%
EW_16	5.96,10.25,7	26.20	22.24	-3.96	**-15.1%**
WW_16	5.78,10.25,1.05	26.10	22.98	-3.12	-11.9%
AA_16	8.81,10.25,4.44	26.30	23.26	-3.04	-11.6%
Average		26.77	23.19	-3.58	-13.4%

AIR HIGH	Coordinates	Temperature T (°C)		ΔT (°C)	Percent Difference
		Experimental	Numerical		
FL_R_M	0.24,6.165,7.26	25.90	22.52	-3.38	-13.1%
FM_R_MH	0.24,6.9,4.22	25.60	21.68	-3.92	**-15.3%**
FM_R_ML	0.24,5.2,4.22	24.40	21.69	-2.71	-11.1%
FR_R_M	0.24,6.165,1.24	26.30	21.00	-5.30	**-20.1%**
EW_15	5.96,6.165,7	24.50	21.39	-3.11	-12.7%
WW_15	5.78,6.165,1.05	25.10	21.72	-3.38	-13.5%
AA_15	8.81,6.165,4.44	24.60	21.61	-2.99	-12.2%
		25.20	21.66	-3.54	-14.1%

AIR HIGH	Coordinates	Temperature T (°C)		ΔT (°C)	Percent Difference
		Experimental	Numerical		
FL_R_B	0.24,2.1,7.26	23.90	21.70	-2.20	-9.2%
FM_R_BH	0.24,3.05,4.22	23.90	21.49	-2.41	-10.1%
FM_R_BL	0.24,3.05,4.22	23.40	21.10	-2.30	-9.8%
FR_R_B	0.24,2.1,1.24	23.00	20.53	-2.47	-10.7%
EW_14	5.96,2.1,7	24.00	20.90	-3.10	-12.9%
WW_14	5.78,2.1,1.05	22.30	20.77	-1.53	-6.8%
AA_14	8.81,2.1,4.44	23.00	21.13	-1.87	-8.1%
		23.36	21.09	-2.27	-9.7%

Table 2: Air Temperatures: Comparison Between Experimental [Basarir 2009 (1)] and Present Numerical Data

It can be noticed from Table 2 that temperatures in the experiment and simulations are in close agreement. In particular, the temperatures remain low near the floor and increase with height. Velocities show similar trends, indicating a period of stagnation near the center of the room which is surrounded by the circulating air.

Chapter 8

Conclusions

The goal of the work presented in this thesis has been to assess the modeling requirements and accuracy of CFD computations using RANS equations for forced-, free- and mixed convection flows in 3-D building enclosures. The CFD simulation software FLUENT 12.1 is employed for this purpose. In order to determine the modeling requirements and accuracy of the RANS simulations, the experimental test data is used for validation of computation.

In Chapter 3, forced convection flow in a 2-D cavity is considered. The influence of mesh size and turbulence models on the accuracy of the solution was evaluated by comparing the computations with the experimental data of Restivo (1979). It was concluded that a mesh size containing between 150000-700000 nodes may be considered sufficient for obtaining solutions with acceptable engineering accuracy. While the solutions with a greater number of nodes are slightly more accurate, they require significantly greater computational time. Between the two (k-ε realizable and k-ω SST) turbulence models employed, it was found that both models produced satisfactory results; however, the k-ε realizable model was slightly better in overall accuracy.

In Chapter 4, the accuracy of the two turbulence models was examined for computing natural convection in a tall, vertical rectangular cavity. The solution mesh contained 165680 nodes. The computations were compared with the experimental data of Bokhari and Betts (2000). It was found that the k-ω SST model provided slightly better correlation with the experimental data than the k-ε realizable model for this case.

In Chapter 5, the accuracy of the two turbulence models was examined again for mixed convection flow for a square cavity. The solution had 173056 nodes. Computations were compared with the experimental data of Blay et al. (1992). It was discovered that

the k-ε realizable model gave slightly better correlation with the experimental data than the k-ω SST model for this case.

The 2-D simulation cases reported in Chapters 3-5 served as the validation cases for the CFD software and provided guidelines about the mesh size and turbulence models that should be employed for obtaining solutions of acceptable engineering accuracy.

In Chapter 6, a 3-D room with natural ventilation has been modeled; this configuration corresponds to the experimental model studied by Jiang and Chen (2003). A mesh with 184992 nodes was used in this simulation. Based on our experience with the k-ω SST model in natural convection flow in Chapter 4, this model was employed in our CFD simulation. The computations for velocity and temperature profiles in various regions of the room shared qualitative agreement with the experimental data. Good quantitative comparisons could not be obtained because of lack a of detailed information about the flow conditions and other parameters from the experiment (e.g. the information about the surface heater temperature). Nevertheless, the CFD simulations were satisfying.

Finally in Chapter 7, the flow field inside an atrium was computed; the experiment data for the atrium was obtained by Basarir (2009). Since the flow in the atrium represents a mixed convection flow with solar radiation, the k-ε realizable model was employed in the simulation based on our experience with 2-D simulation of mixed convection in Chapter 5. The number of nodes used in simulation was 844584. On the whole, good comparison between the computation and experiment was obtained for the velocity and temperatures inside the atrium. The maximum discrepancy between the computations and experiments was 10-15%, depending on the region inside the atrium. In many parts of the atrium, the agreement between computation and experiment was excellent, within 0.5% of each other. It is surmised that a finer mesh will improve the accuracy of CFD predictions in regions where there is greater discrepancy.

In summary, it is demonstrated in this thesis that CFD can model the flow field and heat transfer in building enclosures quite accurately with a proper choice of mesh density and the turbulence model.

Chapter 9

Future Work

1. The cause of significant discrepancy between the numerical simulation and the experimental data in the 3-D natural ventilation reported in Chapter 6 should be further investigated both experimentally and numerically. It appears that it may be worth repeating the experiment to generate good data for CFD validation.

2. Further grid refinement of the atrium model developed in Chapter 7 is needed, in order to correct for the 10-15% underestimation of the ambient air temperature within the atrium in the computation when compared to the experimental data.

3. Additional simulations should be conducted using other turbulence models, including the different variations of the k-ε and k-ω models. Some models, such as the Spalart-Allmaras (S-A) model, were not employed since they require prior knowledge of turbulence length scales within the room (Daiber 2011). Others models, such as the transition k-kl-ω models, may be considered for future study.

References

[1]   Basarir, M. *Numerical Study of the Airflow and Temperature Distributions in an Atrium.*
        Master's thesis, Queen's University, 2009.

[2]   Betts, P.L. and Bokhari, I.H., 2000, "Experiments on turbulent natural
        convection in an enclosed tall cavity," *International Journal of Heat and Fluid Flow*,
        vol. 21, pp. 675-683.

[3]   D. Blay, S. Mergui, and C. Niculae, Confined turbulent mixed convection in the
        presence of a horizontal buoyant wall jet, *Fundamentals of Mixed Convection,
        ASME HTD,* vol. 213, pp. 65-72, 1992.

[4]   Cebeci, T. and Cousteix, J., 2005, *Modeling and Computation of Boundary-Layer Flows:
        Laminar, Turbulent and Transitional Boundary Layers in Incompressible and Compressible
        Flows*, Horizons Publishing Inc., California

[5]   Cornell University. "FLUENT Learning Modules," Ithaca, NY, 2011. Oct
        2011.
        <https://confluence.cornell.edu/display/SIMULATION/FLUENT+Learning
        +Modules>

[6]   Currie, I. G., 2003, *Fundamental Mechanics of Fluids*, Taylor and Francis Group,
        Florida

[7]   Daiber, J. *Increasing Energy Efficiency of HVAC Systems in Buildings Using Phase
        Change Material.* Master's thesis, Washington University in St. Louis, 2011.

[8]   de Villiers, E. "Climate control and HVAC simulation for occupied spaces,
        implementation and validation" (presentation at 5th OpenFOAM Workshop,
        Chalmers, Gothenburg, Sweden) 21 Jun 2010.

[9]   FLUENT Documentation, 2009, ANSYS, Inc.

[10]   Horikiri, K., Yao, Y., and Yao, J., 2011, "Numerical simulation of convective
        airflow in an empty room," *International Journal of Energy and Environment*, Vol. 5,
        pp. 574-581.

[11]   International Energy Agency, 2011, "Energy Balances of OECD Countries."

[12]   Jiang, Y. and Chen, Q., 2003, "Buoyancy-driven single-sided natural ventilation
        in buildings with large openings," *International Journal of Heat and Mass Transfer*,
        vol. 46, pp. 973-988.

[13] Jiang, Y. E-mail to Alex Kayne, 4 Apr 2012.

[14] McQuiston, F., Parker, J., and Spitler, F., *Heating, Ventilating, and Air Conditioning: Analysis and Design*, John Wiley and Sons, 2005.

[15] Menter, F.R., Kuntz, M., and Langtry, R., 2003, "Ten years of industrial experience with the SST turbulence model," *Turbulence, Heat and Mass Transfer*, vol. 4.

[16] Pérez-Lombard, L., Ortiz J., and Pout, C., 2008, "A review on buildings energy consumption information," *Energy and Buildings*, vol. 40, pp. 394-398

[17] Restivo, A. Turbulent flow in ventilated rooms. Ph. D. dissertation, University of London, U.K. (1979).

[18] U.S. Energy Information Administration. "Summary Statistics for the United States, 1999-2010," Washington D.C. 2010. Web. 13 Mar 2012. <http://205.254.135.7/electricity/annual/>

[19] U.S. Environmental Protection Agency. "The Inside Story: A Guide to Indoor Air Quality," Washington D.C. 1995. Web. 4 Apr 2012. <http://www.epa.gov/iaq/pubs/insidestory.html>

[20] Zuo, W. and Chen, Q., 2009, "Real time or faster-than-real-time simulation of airflow in buildilngs," *Indoor Air*, vol. 19, pp. 33-34.

Vita

Alexander Kayne

Date of Birth   October 7, 1988

Place of Birth   Carbondale, Illinois

Degrees   B.S. Physics, June 2010
M.S. Mechanical Engineering, May 2012

May 2012

CFD Modeling of Convection Flows,   Kayne, M.S. 2012